



Science Arts & Métiers (SAM)

is an open access repository that collects the work of Arts et Métiers Institute of Technology researchers and makes it freely available over the web where possible.

This is an author-deposited version published in: <https://sam.ensam.eu>
Handle ID: <http://hdl.handle.net/10985/10159>

To cite this version :

F. PABLO, O. POLIT, Frédéric DAU - New reference solutions and parametrics study for multilayered cylindrical shell - International Journal of research and Reviews in Applied Sciences - Vol. 4, n°2, p.133-161 - 2012

Any correspondence concerning this service should be sent to the repository

Administrator : scienceouverte@ensam.eu



NEW REFERENCE SOLUTIONS AND PARAMETRIC STUDY FOR MULTILAYERED CYLINDRICAL SHELL

F. Dau^{1*}, F. Pablo² & O. Polit²

¹LAMEFIP - ENSAM - Esplanade des arts et métiers - 33405 Talence - France

²LMpX - Univ. Paris X - 1 Chemin Desvallières - 92410 Ville d'Avray - France

Email : frederic.dau@lamef.bordeaux.ensam.fr

ABSTRACT

This work deals with the performances of a refined shell model for modeling cylindrical multilayered deep or shallow, thin or thick shells. To this end, new 3D analytical solutions are built from the well known Ren cylindrical shell panel and stand for reference solutions. Next, a parametric study varying the shell geometry (radius of curvature, thickness, curve side length of the panel) and the number of layers is carried out numerically using a C^1 finite element based on the present shell model. Numerical results are then compared to the new set of reference solutions established for laminates of 1, 2, 3 and 5 layers. Finally, use restrictions according to the shell geometry can be done. Moreover, indications about shell curvature can be obtained considering the ratio between radius and curve length.

Keywords: *multilayered shells, reference solutions, refined shell model, geometrical, parametric study, interlayer continuity conditions, C^1 finite element.*

1. INTRODUCTION

Due to their exceptional specific stiffness and strength, composite materials are being increasingly used in advanced structural applications. Numerous computational models dedicated to multilayered plates and shells analysis have been developed; see [1–4]. A large part of models is dedicated to high-order theories [5–8] and zig-zag theories see the historical review paper [9], allowing suitable transverse shear effects representation. Based on previous models, finite elements have been elaborated to assess accurate displacement, strain and stress values for an efficient structural design; the following papers can be consulted for plate and shell finite element [10–15] but also hybrid solid-shell or 3D finite element [16–19].

In the present work, a refined shell model called sinus model is considered. A cosine transverse shear distribution satisfying both displacements and transverse shear stress continuities at interlayer and at free faces is assumed in this model. The associated C^1 finite element [15,20] is used to perform the parametric study about thick-ness (from thin to thick), curvature (from shallow to deep), see Fig. 1, and lamination scheme of cylindrical panels. The main objective is to evaluate the range of validity for this high order model when geometrical Love [21,22] and Donnell [23,24] assumptions are introduced in the strain field. To this end, new '3D' reference solutions are proposed based on Ren's work [25].

After some geometrical considerations on shells, the refined sinus model is recalled and simplified strain expressions taking into account the geometrical hypotheses are presented. Secondly, cylindrical panel test configuration is reminded pointing out geo-metrical parameters kept for this study. New reference solutions for different geometrical parameters and stacking sequence are then obtained. In the following section, the parametric study is performed using the C^1 6-node triangular shell finite element [15]. A homogeneous cylindrical panel is first considered. Results issued from different simplified strain field are compared with the new reference solutions so to select the most reliable model suitable for shallow to deep and thin to thick cylindrical shells. Multilayered cylindrical panels are then simulated using the selected model. Comparisons with reference solutions but also with Classical Shell Theory (CST) and First-order Shear Deformation Theory (FSDT) are then given, deducing the relevance of geometrical hypotheses for this refined shell model. Concluding remarks are finally proposed in the last section.

2. GEOMETRIC CONSIDERATIONS ON SHELL

A shell C with a middle surface S and a constant thickness e is defined by, see [26]:

$$C = \left\{ M \in \mathcal{R}^3 : \overrightarrow{OM}(\xi, z = \xi^3) = r(\xi^1, \xi^2, z) = \Phi(\xi) + z\mathbf{a}_3; \xi \in \Omega; -\frac{1}{2}e(\xi) \leq z \leq \frac{1}{2}e(\xi) \right\}$$

where the middle surface is described by a map Φ from a parametric bi dimensional domain Ω as:

$$\begin{aligned} \Phi & : \Omega \subset \mathcal{R}^2 \longrightarrow \mathcal{S} \subset \mathcal{R}^3 \\ \xi = (\xi^1, \xi^2) & \longmapsto \Phi(\xi) \end{aligned} \tag{1}$$

For example, a cylindrical panel is obtained from the parametric space (ξ^1, ξ^2) using Eq. (2) and the map is represented on Fig. 2.

$$(\xi^1, \xi^2) \rightarrow \begin{cases} X(\xi^1, \xi^2) = R \sin \frac{\xi^1}{R} \\ Y(\xi^1, \xi^2) = \xi^2 \\ Z(\xi^1, \xi^2) = R \cos \frac{\xi^1}{R} \end{cases} \tag{2}$$

For a point on the shell middle surface, covariant base vectors are usually obtained as follows:

$$\mathbf{a}_\alpha = \Phi(\xi^1, \xi^2)_{,\alpha} \quad ; \quad \mathbf{a}_3 = \frac{\mathbf{a}_1 \times \mathbf{a}_2}{\|\mathbf{a}_1 \times \mathbf{a}_2\|} = \mathbf{t}_3$$

In Eq.(3) and further on, latin indices i, j, \dots take their values in the set $\{1, 2, 3\}$ while greek indices α, β, \dots take their values in the set $\{1, 2\}$. The summation convention on repeated indices and the classic notation $(\)_{,\alpha} = \partial(\) / \partial \xi^\alpha$ are used. For any point of the shell, covariant base vectors are now deduced as:

$$\mathbf{g}_\alpha = r(\xi^1, \xi^2, z)_{,\alpha} = (\delta_\alpha^\beta - z b_\alpha^\beta) \mathbf{a}_\beta = \mu_\alpha^\beta \mathbf{a}_\beta \quad \text{and} \quad \mathbf{g}_3 = \mathbf{a}_3 \tag{4}$$

The mixed tensor m^β_α must be also introduced:

$$m^\beta_\alpha = (\mu^{-1})^\beta_\alpha = \frac{1}{\mu} \{ \delta_\alpha^\beta + z(b_\alpha^\beta - 2H\delta_\alpha^\beta) \} \tag{5}$$

$$\text{where } \mu = \det(\mu_\alpha^\beta) = 1 - 2Hz + (z)^2 K \quad ; \quad H = \frac{1}{2} \text{tr}(b_\alpha^\beta) \quad ; \quad K = \det(b_\alpha^\beta).$$

Therefore, the covariant metric tensor $a_{\alpha\beta}$, covariant $b_{\alpha\beta}$ and mixte b^β_α curvature tensors can be deduced. These tensors and some relations between them are recalled hereafter:

$$\begin{aligned} a_{\alpha\beta} = a_{\beta\alpha} = \mathbf{a}_\alpha \cdot \mathbf{a}_\beta \quad \mathbf{a}_\alpha = a_{\alpha\beta} \mathbf{a}^\beta \quad a = \det(a_{\alpha\beta}) \\ b_{\alpha\beta} = b_{\beta\alpha} = -\mathbf{a}_\alpha \cdot \mathbf{a}_{3,\beta} \quad b^\beta_\alpha = a^{\beta\gamma} b_{\gamma\alpha} \end{aligned} \tag{6}$$

Finally, the elementary surface and volume, respectively dS and dV are classically given by:

$$\begin{aligned} dS & = \sqrt{a} d\xi^1 d\xi^2 \\ dV & = \mu dS dz \end{aligned} \tag{7}$$

All these classic relations as well as more details for obtaining the Christoffel symbols and other differential geometrical entities can be found in Bernadou [26].

3. THE REFINED SHELL MODEL AND STRAIN FIELD SIMPLIFICATIONS

3.1 The displacement field

The refined displacement field is based on an assumed transverse shear stress distribution (as introduced in Whitney's work [27]) developed in [11] and extended in [20,15]. The classical plate/shell assumptions $\sigma_{33} = 0$ is used. Continuity requirements for both displacements and transverse shear stresses at inter layers and at free faces are satisfied. The main steps of the procedure are summarized in Appendix A. For a layer (k), the displacement field components are expressed in the \mathbf{a} contravariant basis by:

$$\begin{cases} u_1^{(k)}(\xi^1, \xi^2, z, t) = \mu_1^\alpha v_\alpha(\xi^1, \xi^2, t) - z v_{3,1}(\xi^1, \xi^2, t) + F_1^{\alpha(k)}(z) \gamma_\alpha^0(\xi^1, \xi^2, t) \\ u_2^{(k)}(\xi^1, \xi^2, z, t) = \mu_2^\alpha v_\alpha(\xi^1, \xi^2, t) - z v_{3,2}(\xi^1, \xi^2, t) + F_2^{\alpha(k)}(z) \gamma_\alpha^0(\xi^1, \xi^2, t) \\ u_3^{(k)}(\xi^1, \xi^2, z, t) = v_3(\xi^1, \xi^2, t) \end{cases} \quad (8)$$

where t is the time and classical summation on repeated indices is used. In Eq. (8),

- v_i are the displacements of a point on the middle surface;
- γ_α^0 is the transverse shear strain at $z=0$ defined by

$$\gamma_\alpha^0 = \beta_\alpha + b_\alpha^\beta v_\beta + v_{3,\alpha}$$

- where $\beta_1 = \theta_2$ and $\beta_2 = -\theta_1$, being θ_1 and θ_2 the positive material fiber rotations about the \mathbf{a}^1 and \mathbf{a}^2 axis, respectively.
- $F_\beta^{\alpha(k)}(z)$ are functions of the normal transverse co-ordinate z defining the distribution of the transverse shear stresses through the thickness. They are expressed by:

$$\begin{aligned} F_1^{1(k)}(z) &= f_1(z) + g_1^{(k)}(z); & F_1^{2(k)}(z) &= g_2^{(k)}(z) \\ F_2^{1(k)}(z) &= g_3^{(k)}(z); & F_2^{2(k)}(z) &= f_2(z) + g_4^{(k)}(z) \end{aligned} \quad (9)$$

In Eq. (9), the thickness functions $f_1, f_2, g_1^{(k)}, \dots, g_4^{(k)}$ depend on the coefficients $a_i^{(k)}, d_i^{(k)}, b_{44}, b_{55}$ and on the trigonometric functions as follows:

$$\begin{aligned} f_1(z) &= f(z) - \frac{e}{\pi} b_{55} f'(z) \\ f_2(z) &= f(z) - \frac{e}{\pi} b_{44} f'(z) \\ g_i^{(k)}(z) &= a_i^{(k)} z + d_i^{(k)} \quad i = 1, 2, 3, 4 \text{ and } k = 1, 2, 3, \dots, N. \end{aligned} \quad (10)$$

where $f(z) = e/\pi \sin(\pi z/e)$ and N represents the number of layers. Fig. 3 illustrates the multilayered shell.

The coefficients $a_i^{(k)}, d_i^{(k)}$ on the one hand and b_{44}, b_{55} on the other hand, are determined from the boundary conditions on the top and bottom faces of the shell and from both displacements and transverse shear stresses continuity at interlayers, see Appendix A.

The refined displacement field, see Eq. (8), can be seen as a high order development with respect to the transversal z co-ordinate. Classical shell models can be retrieved using $f_1, f_2, g_1^{(k)}, \dots, g_4^{(k)}$ functions as follows:

- Kirchhoff-Love Koiter model (KL-K), called Classical Shell Theory (CST), is obtained with $f_1(z) = f_2(z) = 0$ and $g_i^{(k)}(z) = 0$:

$$\begin{cases} u_1 = \mu_1^\beta v_\beta - z v_{3,1} \\ u_2 = \mu_2^\beta v_\beta - z v_{3,2} \\ u_3 = v_3 \end{cases} \quad (11)$$

– Reissner-Mindlin Nagdhi model (RM-N), called First Order Shear Deformation Theory (FSDT), is obtained by setting $f_1(z) = f_2(z) = z$ and $g_i^{(k)}(z) = 0$:

$$\begin{cases} u_1 = v_1 + z \beta_1 \\ u_2 = v_2 + z \beta_2 \\ u_3 = v_3 \end{cases} \quad (12)$$

Hereafter, the superscript (k) for $u_a^{(k)}$ is omitted in order to lighten the strain field expressions and the finite element description of the model.

3.2 The general strain field

The general strain field directly issued from Eq. (8) is first presented using the total Green-Lagrange formulation. Simplified strain models based on specific geometrical assumptions are subsequently proposed. The resulting models will be assessed in Section 5.

The linear strain components can be expressed in the covariant \mathbf{g}_i basis as:

$$\begin{cases} 2 \tilde{\epsilon}_{\alpha\beta} = \mathbf{g}_\alpha \cdot \mathbf{u}_{,\beta} + \mathbf{g}_\beta \cdot \mathbf{u}_{,\alpha} \\ 2 \tilde{\epsilon}_{\alpha 3} = \mathbf{g}_\alpha \cdot \mathbf{u}_{,3} + \mathbf{g}_3 \cdot \mathbf{u}_{,\alpha} \end{cases} \quad (13)$$

where \mathbf{u} is the displacement vector. Using differential geometrical considerations see Section 2, and after some algebraic calculations, the covariant strain tensor components are obtained in the local contravariant basis \mathbf{a}^i as follows:

$$\begin{aligned} \epsilon = \epsilon_{ij}(a^i \otimes a^j) \quad \text{with} \\ 2\epsilon_{\alpha\beta} = \frac{1}{\mu} \left(\epsilon_{\alpha\beta}^0 + \epsilon_{\beta\alpha}^0 + F_\alpha^\nu(z) \epsilon_{\nu\beta}^1 + F_\beta^\nu(z) \epsilon_{\nu\alpha}^1 + G_\alpha^\nu(z) \epsilon_{\nu\beta}^2 + G_\beta^\nu(z) \epsilon_{\nu\alpha}^2 \right. \\ \left. + z \left\{ (b_\beta^\lambda - 2H\delta_\beta^\lambda) (\epsilon_{\alpha\lambda}^0 + F_\alpha^\nu(z) \epsilon_{\nu\lambda}^1 + G_\alpha^\nu(z) \epsilon_{\nu\lambda}^2) + \right. \right. \\ \left. \left. (b_\alpha^\lambda - 2H\delta_\alpha^\lambda) (\epsilon_{\beta\lambda}^0 + F_\beta^\nu(z) \epsilon_{\nu\lambda}^1 + G_\beta^\nu(z) \epsilon_{\nu\lambda}^2) \right\} \right) \\ 2\epsilon_{\alpha 3} = \frac{1}{\mu} \left(F_\alpha^{\nu'}(z) \gamma_\nu^0 + b_\alpha^\nu (F_\nu^\beta(z) - zF_\nu^{\beta'}(z)) \gamma_\beta^0 \right. \\ \left. + z(b_\alpha^{\nu'} - 2H\delta_\alpha^{\nu'}) \left\{ F_\nu^{\beta'}(z) \gamma_\beta^0 + b_\nu^\beta (F_\beta^\lambda(z) - zF_\beta^{\lambda'}(z)) \gamma_\lambda^0 \right\} \right) \end{aligned} \quad (14)$$

where $G_\alpha^\nu(z) = F_\alpha^\nu(z) - \delta_\alpha^\nu z$

For convenience, the following notation has been introduced in Eq. (14) to separate the characteristic contributions :

$$\begin{aligned} \text{membrane strain :} \quad & \epsilon_{\alpha\beta}^0 = v_{\alpha|\beta} - b_{\alpha\beta} v_3 \\ \text{bending strain 1 :} \quad & \epsilon_{\alpha\beta}^1 = \beta_{\alpha|\beta} \\ \text{bending strain 2 :} \quad & \epsilon_{\alpha\beta}^2 = b_\alpha^\lambda v_{\lambda|\beta} + b_{\alpha|\beta}^\lambda v_\lambda + v_{3|\alpha\beta} \\ \text{transverse shear strain :} \quad & \gamma_\alpha^0 = \beta_\alpha + b_\alpha^\beta v_\beta + v_{3,\alpha} \end{aligned} \quad (15)$$

where symbol ${}_{|\beta}$ stands for the covariant derivative with respect to the curvilinear co-ordinate ξ^β . Furthermore, it is noted that the CST model gives $F_\alpha^\beta(z) = 0$ and $G_\alpha^\beta(z) = z \delta_\alpha^\beta$ with bending strain reduced to $\epsilon_{\alpha\beta}^2$. The FSDT model yields $F_\alpha^\beta(z) = z$ and $G_\alpha^\beta(z) = 0$ and the bending strain is represented by $\epsilon_{\alpha\beta}^1$.

3.3 The strain field simplifications

The general strain field Eq. (14) is now simplified taking into account geometrical properties of the shell. The simplifications are shown to mainly affect the expression for the membrane-bending strains $\epsilon_{\alpha\beta}$. For transverse shear strain expressions $\epsilon_{\alpha 3}$ only the first term $F_{\alpha}^{\nu'}(z)\gamma_{\nu}^0$ is retained according to the continuity requirements, see Appendix A.

The following three strain models can be directly derived from the general one:

SIN-C model (SINus model with Continuity): the membrane-bending strains are not changed while the transverse shear strains are reduced to the first order term, so:

$$\begin{aligned}
 2\epsilon_{\alpha\beta} &= \frac{1}{\mu} \left(\epsilon_{\alpha\beta}^0 + \epsilon_{\beta\alpha}^0 + F_{\alpha}^{\nu}(z)\epsilon_{\nu\beta}^1 + F_{\beta}^{\nu}(z)\epsilon_{\nu\alpha}^1 + G_{\alpha}^{\nu}(z)\epsilon_{\nu\beta}^2 + G_{\beta}^{\nu}(z)\epsilon_{\nu\alpha}^2 \right. \\
 &\quad \left. + z \left\{ (b_{\beta}^{\lambda} - 2H\delta_{\beta}^{\lambda}) (\epsilon_{\alpha\lambda}^0 + F_{\alpha}^{\nu}(z)\epsilon_{\nu\lambda}^1 + G_{\alpha}^{\nu}(z)\epsilon_{\nu\lambda}^2) + \right. \right. \\
 &\quad \left. \left. (b_{\alpha}^{\lambda} - 2H\delta_{\alpha}^{\lambda}) (\epsilon_{\beta\lambda}^0 + F_{\beta}^{\nu}(z)\epsilon_{\nu\lambda}^1 + G_{\beta}^{\nu}(z)\epsilon_{\nu\lambda}^2) \right\} \right) \\
 2\epsilon_{\alpha 3} &= F_{\alpha}^{\nu'}(z)\gamma_{\nu}^0
 \end{aligned} \tag{16}$$

SIN-C/L model (SINus model with Continuity and Love hypothesis): this model is associated with the shallow shell hypothesis introduced by Love [21] using the following geometrical assumption:

$$zb_{\alpha}^{\beta} \ll 1 \iff 1 \pm zb_{\alpha}^{\beta} \sim 1$$

Therefore, the membrane-bending strains become:

$$\begin{aligned}
 2\epsilon_{\alpha\beta} &= \epsilon_{\alpha\beta}^0 + \epsilon_{\beta\alpha}^0 + F_{\alpha}^{\nu}(z)\epsilon_{\nu\beta}^1 + F_{\beta}^{\nu}(z)\epsilon_{\nu\alpha}^1 + G_{\alpha}^{\nu}(z)\epsilon_{\nu\beta}^2 + G_{\beta}^{\nu}(z)\epsilon_{\nu\alpha}^2 \\
 2\epsilon_{\alpha 3} &= F_{\alpha}^{\nu'}(z)\gamma_{\nu}^0
 \end{aligned} \tag{17}$$

Furthermore, the bending strain 2 expression becomes:

$$\epsilon_{\alpha\beta}^2 = v_{3|\alpha\beta}$$

SIN-C/L-D model (SINus model with Continuity and Love-Donnell hypothesis): in this model, Donnell's assumptions for which the membrane coupling effects in the transverse shear strain at the middle surface are neglected, are introduced into the SIN-C/L model. The following plate transverse shear strain components are then used:

$$\gamma_{\alpha}^0 = \beta_{\alpha} + v_{3,a}$$

A synthesis of the strain expressions for the three models is given in Table 1.

4. REN CYLINDRICAL PANEL: new 3D reference solutions

The cylindrical panel test configuration of Ren is recalled in Fig. 4. Reference elastic solutions, see [25], are given for a homogeneous and a three layers shells with $R/a = 3/\pi$ and $S = R/e = 4, 10, 50, 100$. In this work, reference elastic solutions are extended to other shells with different ratios $R/a, R/e$ (see Fig. 5) and for other lamination schemes.

The configurations of the shell panel considered in this study are described below.

Shell geometry (see Fig. 5):

- $\zeta^1 \in [0, R\Phi]$ and the panel is assumed to be infinite along the ζ^2 direction. Three values of Φ angle are considered: $\Phi = 30^\circ, 60^\circ, 120^\circ$;
- middle radius R is equal to 10;

- the curvature of the shell is controlled by the ratio $R/a = 1/\Phi$ where a is the length of the curve side. The smaller R/a ratio is, the deeper is the shell. For the parametric study, the ratio R/a takes the values $6/\pi$, $3/\pi$, $3/2\pi$, corresponding to an angle Φ equal to 30° , 60° , 120° , respectively;
- the thickness e of the shell is controlled by the ratio $S = R/e$, the shell is all the thinner as S ratio is high. Ratios $S = R/e = 4, 10, 50, 100$ are considered for this study.

Material properties:

one layer 0° , two layers $(0^\circ, 90^\circ)$, three layers $(0^\circ, 90^\circ, 0^\circ)$ and five layers $(0^\circ, 90^\circ, 0^\circ, 90^\circ, 0^\circ)$ of equal thickness are considered with the Pagano material properties [28]:

$$E_1 = 25E_2 ; G_{12} = G_{13} = 0.5E_2 ; G_{23} = 0.2E_2 ; \nu_{12} = 0.25$$

Loading and boundary conditions:

A sinusoidal pressure with respect to ζ^1 is applied: $q(\zeta^1) = q_1 \sin(\pi\zeta^1/R\Phi)$ where q_1 is the maximum pressure value. The cylindrical panel is simply supported along its straight edges.

The methodology to obtain analytical solutions based on the plane strain hypothesis is detailed in Appendix B. These analytical solutions, mentioned in bold character in tables 2 to 5, are taken as reference for the parametric study presented in the following section.

5. THE PARAMETRIC STUDY

The different approximations for the strain field introduced in Section 3 are evaluated by means of a six node triangular FE. The main characteristics of this finite element, see [20,29], are briefly recalled. Using a conforming finite element approach, the displacement field given by Eq. (8) indicates that v_3^h must be a C^1 -continuous function. The other generalized displacements v_α^h and θ_α^h have to be defined in the Sobolev space $H^1(\Omega_\alpha)$ and be at least C^0 -continuous.

Therefore, we choose the Argyris interpolation [30] for the deflection and the Ganev interpolation [31] for the other generalized displacements. Note that the Argyris interpolation is exactly of continuity C^1 and the Ganev interpolation involves a semi- C^1 continuity which is not needed here. The long expressions for these interpolations are omitted here, and the reader is referred to either the original papers [30] and [31] or to the book of Bernadou [26].

The degrees of freedom (dof) associated with one finite element in the local curvilinear basis are given as:

- for a corner node:

$$\begin{matrix} v_1 & v_{1,1} & v_{1,2} & v_2 & v_{2,1} & v_{2,2} \\ v_3 & v_{3,1} & v_{3,2} & v_{3,11} & v_{3,22} & v_{3,12} \\ \theta_1 & \theta_{1,1} & \theta_{1,2} & \theta_2 & \theta_{2,1} & \theta_{2,2} \end{matrix} \quad (18)$$

- while, for a mid-side node:

$$\begin{matrix} v_1 & v_{1,n} & v_2 & v_{2,n} \\ v_{3,n} \\ \theta_1 & \theta_{1,n} & \theta_2 & \theta_{2,n} \end{matrix} \quad (19)$$

where $(\)_{,n}$ indicates the derivative with respect to the normal direction along element edge.

First, simulations on homogeneous case involving different shell geometries (R/a , R/e) are performed. The aim is to evaluate present **SIN** model including Love and Donnell assumptions with respect to analytical reference solutions. Then, the most reliable model for shallow to deep and thin to thick shells is retained. Secondly, multilayered shell panels with 2, 3 and 5-ply are simulated using the selected model. Transverse displacement and stresses are compared with analytical solutions. CST and FSDT solutions, deduced respectively from Eq. (11) and Eq. (12), are also mentioned.

For any case, only a quarter of the panel is modeled and the $N=4$ mesh is retained, see Fig. 7. Non-dimensional absolute values v_3^- , σ_{11}^- and σ_{13}^- are defined by:

$$\begin{aligned}
 \bar{v}_3 &= v_3 E_2 10 / (q_1 e S^4) \\
 \bar{\sigma}_{11} &= \sigma_{11} / (q_1 S^2) \\
 \bar{\sigma}_{13} &= \sigma_{13} / (q_1 S)
 \end{aligned}
 \tag{20}$$

\bar{v}_3 , $\bar{\sigma}_{11}$ and $\bar{\sigma}_{13}$ are respectively evaluated at $(\Phi/2, L/2, 0)$, $(\Phi/2, L/2, +e/2)$ and $(\Phi, L/2, 0)$ and summarized in tables 2 to 5. Relative errors between numerical values and reference solutions are finally given in Fig. 10 to Fig. 15 and Fig. 18. The stresses are computed from the constitutive law. Alternatively, a post-processing computation integrating the 3D equilibrium equations along the thickness has been used.

5.1 Homogeneous case

Results are summarized in Table 2. In this table, the geometry of the shell varies as follows:

– from left to right, the angle Φ is increasing: the shell changes from shallow to deep; – from top to bottom, the thickness e is decreasing: the shell changes from thick to thin.

5.1.1 Discussion on models pertinence according to $S = R/e$ and R/a ratios

The pertinence of the presented models for a shallow shell ($R/a = 6/\pi$), a deep shell ($R/a = 3/(2\pi)$) and a shell with intermediate curvature ($R/a = 3/\pi$) can be assessed by means of the results reported in Fig. 10, Fig. 11 and Fig. 12. Several remarks can be done:

- for $R/a = 6/\pi$, see Fig. 10, all the models give comparable results. Relative errors on $\bar{\sigma}_{11}$ and $\bar{\sigma}_{13}$ are respectively lower than 10% and 5% for all S values. Relative errors on \bar{v}_3 are significant but acceptable (between 12% and 19%) when the shell becomes thick (ratio $S = 4$);
- for $R/a = 3/2\pi$, see Fig. 12, some differences can be noticed on both stresses and transverse displacement:
 - SIN/L-D model is not suitable.
 - SIN/L model presents significant discrepancy on transverse displacement \bar{v}_3 varying from 29% for ratios ($S = 50$, $S = 100$) to 41% for smaller S ratio and also on the transverse shear stress $\bar{\sigma}_{13}$ which is about 16% for ratios ($S = 50$, $S = 100$).
 - SIN model gives best results.
- for intermediate ratio $R/a = 3/\pi$, see Fig. 11, interesting constatations can be done:
 - \bar{v}_3 , $\bar{\sigma}_{11}$ and $\bar{\sigma}_{13}$ estimated values using SIN model are good, whatever ratio S may be.
 - SIN/L model gives smaller discrepancy than those observed for $R/a = 3/2\pi$: less than 17% on the transverse displacement \bar{v}_3 , less than 7% on transverse shear $\bar{\sigma}_{13}$.
 - for SIN/L-D model, \bar{v}_3 , $\bar{\sigma}_{11}$ and $\bar{\sigma}_{13}$ obtained are far from the reference solution. Donnell assumption becomes very penalizing for \bar{v}_3 .

Moreover, results issued from SIN model are presented in Fig. 13 in order to show the homogeneity of its behaviour for all R/a ratios and for $S = R/e$ greater than 4.

5.1.2 Synthesis from parametric study on the homogeneous case

From the previous remarks, we can keep in mind:

- SIN model clearly appears as the best one providing reliable results for all shell geometries;
- indication about shell curvature can be obtained considering ratio R/a . Ratio $R/a \sim 1$ seems to correspond to the limit between a shallow and a deep shell. In that way, ratio $R/a < 1$ rather characterizes a deep shell whereas ratio $R/a > 1$ is characteristic of a shallow shell;
- for shallow shell, good results are obtained by all models when the shell is thin or thick. Love hypothesis, $1 \pm \nu \beta_\alpha \sim 1$, and Donnell one, $\gamma_\alpha^0 = \beta_\alpha + \nu_{3,\alpha}$, can suit in this case.
- Love and Donnell hypothesis cannot be used for deep shells.

In the following, SIN model is conserved including continuity requirements for multilayered case: it is now called SIN-C.

5.2 Multilayered case

5.2.1 Two layers case

Results are summarized in Table 3 and plotted on Fig. 14 for ratios $R/a = 6/\pi, 3/\pi, 3/2\pi$. For this two-layer case, σ_{13}^- is evaluated at $(\Phi, L/2, \theta/4)$ position and not at $(\Phi, L/2, 0)$ one like for others cases. Relative errors on V_3^- and σ_{11}^- remain satisfactory whereas σ_{13}^- relative error does not appear acceptable. In this particular case where the maximum transverse shear stress σ_{13}^- occurs on the middle of the bottom layer but not on the middle shell surface, the prediction of the transverse shear stress by a cosine function through the shell thickness is not very good. Improvements are significant integrating equilibrium equations at post processing level, see Fig. 8.

5.2.2 Three layers case

Comparisons with classical CST and FSDT shell models in Table 4 and on plots Fig. 15 show reliable results obtained using SIN-C model. Relative errors are logically more significant for thick shell ($S=4$) when the shell draws near to a 3D solid.

σ_{11}^- and σ_{13}^- through the thickness distributions are plotted on Fig. 16, Fig. 9, Fig. 17 for ratio $R/a = 3/\pi$ and different ratios S . A good behavior is obtained excepted for $S=4$ where distribution of σ_{13}^- is sensitive to 3D effect, while Sinus model gives always symmetric σ_{13}^- distribution. As seen before, this point can be advantageously improved by integrating the equilibrium equations.

5.2.3 Five layers case

Results are summarized in Table 5 and plotted on Fig. 18. Same constatations as for three-layer case can be done and the homogeneity of the results can also be observed for all ratios R/a . Relative errors obtained remain very acceptable for all tested geometries.

6. CONCLUSION

In this paper, a refined shell model to analyze cylindrical multilayer deep or shallow, thin or thick shells have been evaluated. The effects of the well known Love and Donnell shell hypotheses were particularly looked at in order to evaluate the range of validity of such high order model. To this end, the shell geometry has been restricted to Ren's cylindrical shell panel for which new '3D' reference solutions have been established varying the thickness R/e , the curvature R/a and the number of layers for laminates. Next, a parametric study has been performed numerically using a C^1 6-node triangular finite element based on the present refined shell model and numerical results have been compared to reference solutions.

The parametric study on homogeneous case has revealed that:

- the shell curvature can be measured by the ratio R/a . The $R/a = 3/\pi \sim 1$ seems to be representative of the limit between a shallow and a deep shell;
- Donnell assumption is acceptable only for shallow shells;
- Love assumption $1 \pm \alpha^2 \sim 1$ is not suitable for semi-thick shells and for deep shells;
- the Sinus model provides reliable results for all considered shell geometries.

Furthermore, numerical simulations on multilayered cases have proved that:

- the SIN-C model gives good results for both semi-thick shells ($S > 4$) and deep shells ($R/a < 1$);
- an accurate transverse shear stresses distribution is obtained. In the case of the two layers shell, the use of the equilibrium equations is efficient to recover the distribution but the maximal value of the transverse shear stress is well evaluated using the constitutive law.

REFERENCES

- [1] A. Noor, W. Burton, Assessment of computational models for multilayered composite shells, *App. Mech. Rev.* 43 (4) (1990) 67–97.
- [2] A. Noor, W. Burton, C. Bert, Computational models for sandwich panels and shells, *App. Mech. Rev.* 49 (3) (1996) 155–199.
- [3] E. Carrera, Theories and finite elements for multilayered, anisotropic, composite plates and shells, *Arch. Comput. Meth. Engng.* 9 (2) (2002) 87–140.
- [4] V. G. Piskunov, A. O. Rasskazov, Evolution of the theory of laminated plates and shells, *J. Comp. Materials* 4 (1970) 330–343.
- [5] J. Reddy, C. Liu, A higher-order shear deformation theory of laminated elastic shells, *Int. J. Eng. Sci.* 23 (1985) 319–330.
- [6] M. Touratier, A refined theory of laminated shallow shells, *Int. J. Solids Struct.* 29 (11) (1992) 1401–1415.
- [7] X.-P. Shu, A refined theory of laminated shells with higher order transverse shear deformation, *Int. J. Solids Struct.* 34 (6) (1997) 673–683.
- [8] C. Ossadow, M. Touratier, P. Muller, Deep doubly curved multilayered shell theory, *AIAA J.* 37 (1) (1999) 100–109.
- [9] E. Carrera, Historical review of zig-zag theories for multilayered plates and shells, *App. Mech. Rev.* 56 (2003) 287–308.
- [10] M. D. Sciuva, A third-order triangular multilayered plate finite element with continuous interlaminar stresses, *Int. J. Num. Meth. Eng.* 38 (1995) 1–26.
- [11] A. Béakou, M. Touratier, A rectangular finite element for analysing composite multilayered shallow shells in statics, vibration and buckling, *Int. J. Num. Meth. Eng.* 36 (1993) 627–653.
- [12] P. Gaudenzi, A. Mannini, R. Carbonaro, Multi-layer higher-order finite elements for the analysis of free-edge stresses in composite laminates, *Int. J. Num. Meth. Eng.* 41 (1998) 851–873.
- [13] B. Brank, E. Carrera, A family of shear deformable shell finite elements for composite structures, *Comput. Struct.* 76 (2000) 287–297.
- [14] H. Yang, S. Saigal, A. Masud, R. Kapania, A survey of recent shell finite elements, *Int. J. Num. Meth. Eng.* 47 (2000) 101–127.
- [15] F. Dau, A doubly curved c^1 finite shell element based on a refined model for multilayered/sandwich shell structures, Ph.D. thesis, ENSAM Engineering School, Paris-France (2004).
- [16] S. Klinkel, F. Gruttmann, W. Wagner, A continuum based three dimensional shell element for laminated structures, *Comput. Struct.* 71 (1999) 43–62.
- [17] K. Sze, L. Yao, T. Pian, An eighteen-node hybrid-stress solid-shell element for homogeneous and laminated structures, *Fin. Elem. Anal. Des.* 38 (2002) 353–374.
- [18] K. Y. Sze, Three dimensional continuum finite element models for plate/shell analysis, *Prog. Struct. Eng. Mater.* 4 (2002) 400–407.
- [19] H. Sheng, J. Ye, A three dimensional state space finite element solution for laminated composite cylindrical shells, *Comput. Methods Appl. Mech. Eng.* 192 (2003) 2441–2459.
- [20] F. Dau, O. Polit, M. Touratier, An efficient c^1 finite element with continuity requirements for multilayered/sandwich shell structures, *Comput. Struct.* 82 (2004) 1989–1899.
- [21] A. Love, *A Treatise on the Mathematical Theory of Elasticity*, 4th Edition, Dover Publications, New York, 1944.
- [22] V. Novozhilov, *The theory of thin shells*, Groningen : Noordhoff .
- [23] L. H. Donnell, *Stability of thin walled tubes under torsion*, NACA Report 479 .
- [24] K. M. Mushtari, *On the stability of cylindrical shells subjected to torsion*, Trudy Kazanskego aviatsionnogo inatituta .
- [25] J. G. Ren, Exact solutions for laminated cylindrical shells in cylindrical bending, *Comp. Sci & Tech.* 29 (1987) 169–187.
- [26] M. Bernadou, *Finite Element Methods for Thin Shell Problems*, John Wiley and Sons, 1996.
- [27] J. Whitney, The effect of transverse shear deformation on the bending of laminated plates, *J. Comp. Materials* 3 (1969) 534–547.
- [28] N. Pagano, Exact solutions for rectangular bidirectional composites and sandwich plates, *J. Comp. Materials* 4 (1970) 20–34.
- [29] O. Polit, F. Dau, M. Touratier, C^1 plate and shell finite element for geometrically non-linear analysis of multilayered structures, *Comput. Struct.* 84 (2006) 1264–1274.

- [30] J. Argyris, I. Fried, D. Scharpf, The tuba family of plate elements for the matrix displacement method, *Aero. J. Royal Aeronaut. Soc.* 72 (1968) 701–709.
- [31] H. Ganev, T. Dimitrov, Calculation of arch dams as a shell using an ibm-370 computer and curved finite elements, in: *Theory of shells*, North-Holland, Amsterdam, 1980, pp. 691–696.
- [32] L. Doxsee, A higher order theory of hygrothermal behaviour of laminated composite shells, *Int. J. Solids Struct.* 25 (1989) 339–355.

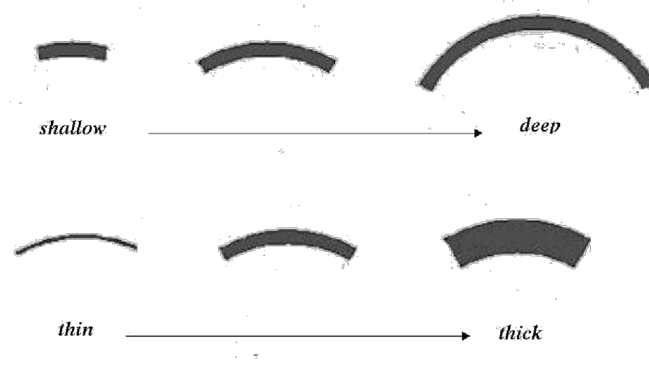


Fig 1. Different geometries for the shell panel

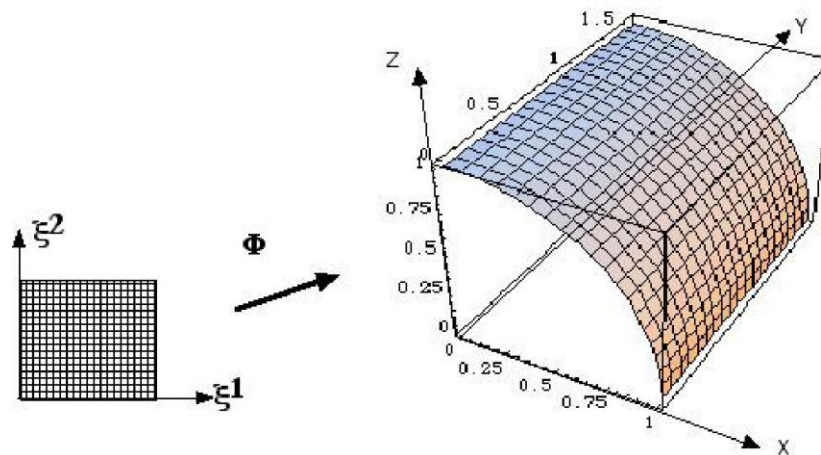


Fig. 2. The bidimensional domain and the shell panel using a geometrical map.

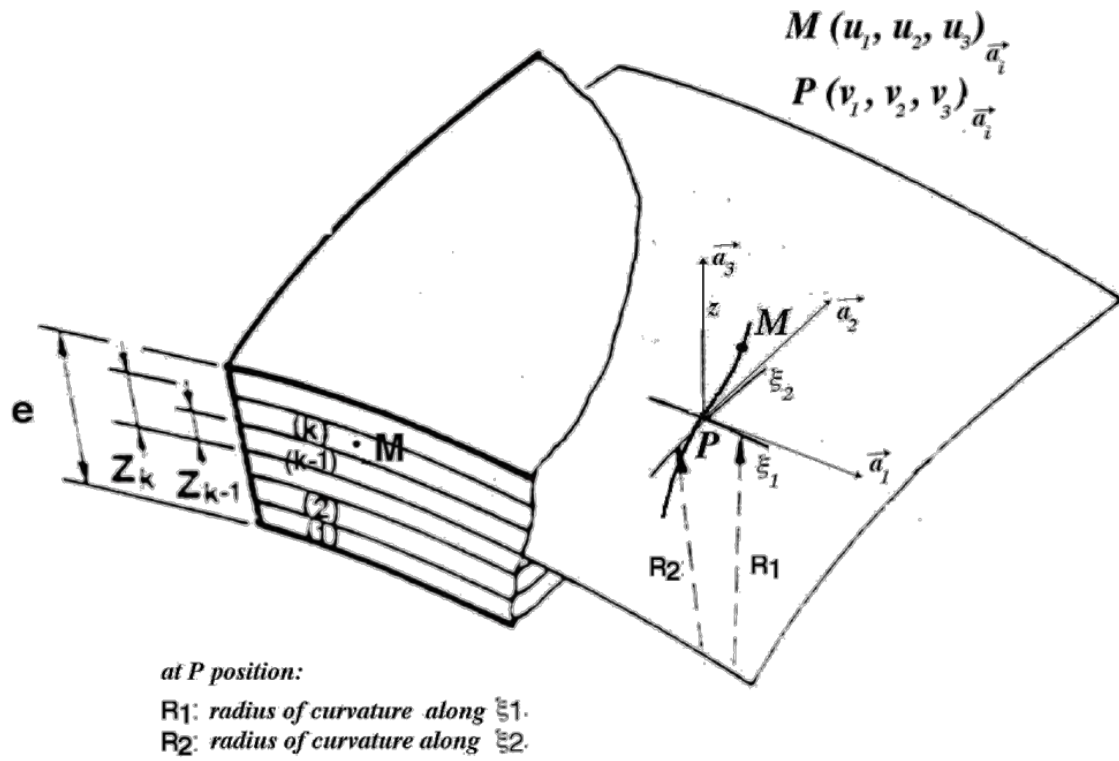


Fig. 3. Laminations and deformed normal material fiber in homogeneous case.

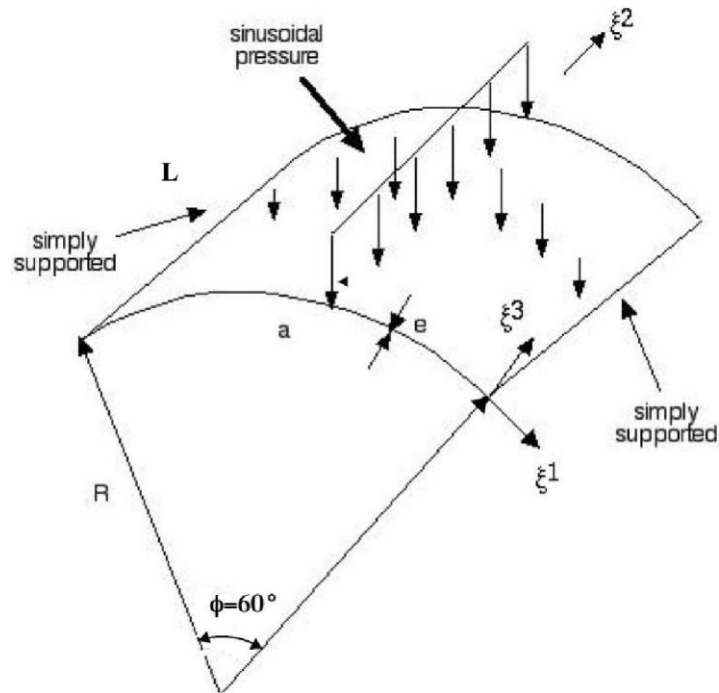


Fig. 4. The Ren laminated cylindrical shell panel - Reference configuration.

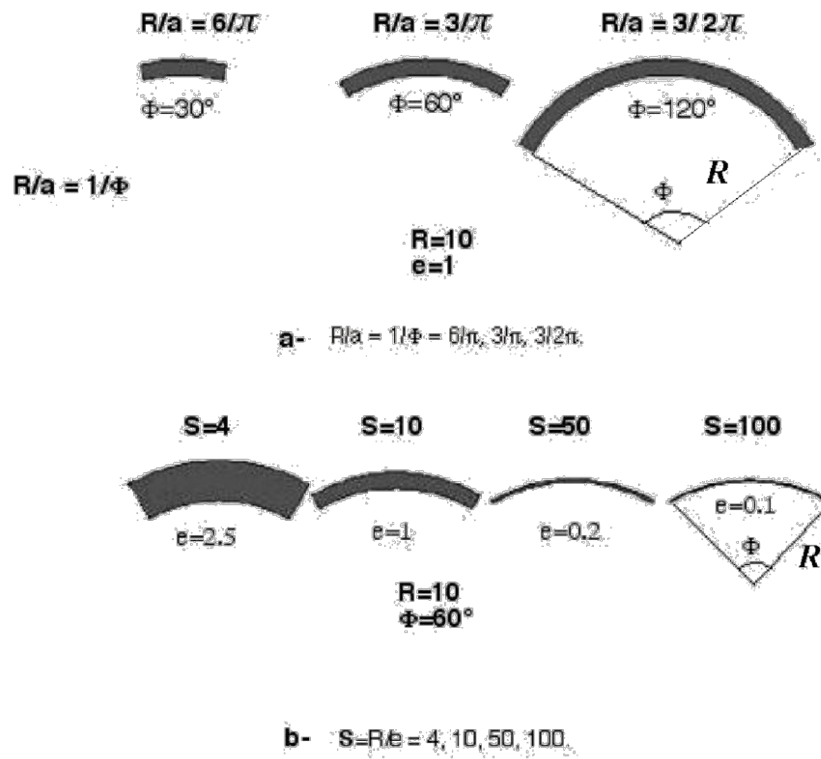


Fig 5. R/e and R/a ratios

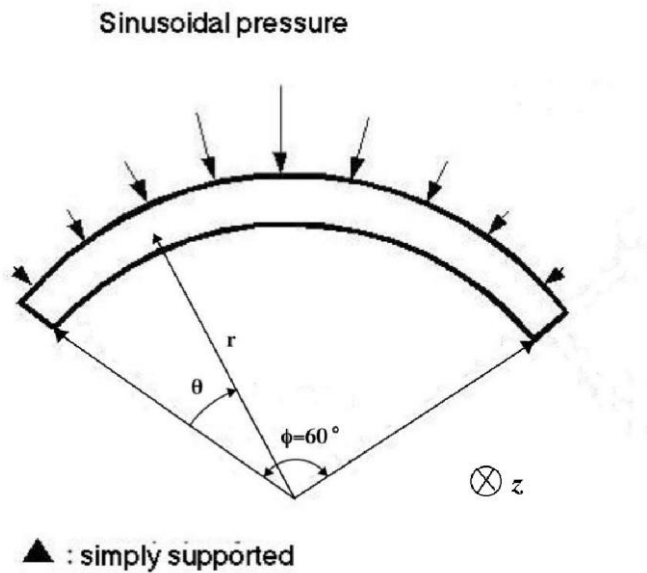


Fig 6. The R_{en} laminated cylindrical shell panel: plane strain state.

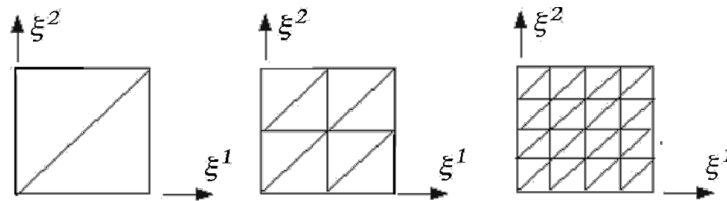


Fig. 7. Meshes in parametric space.

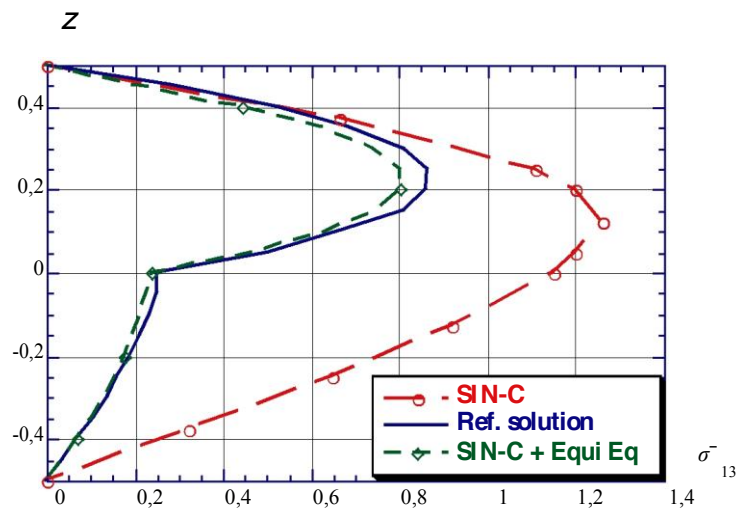


Fig. 8. Two layers case - Comparison of σ^-_{13} distribution.

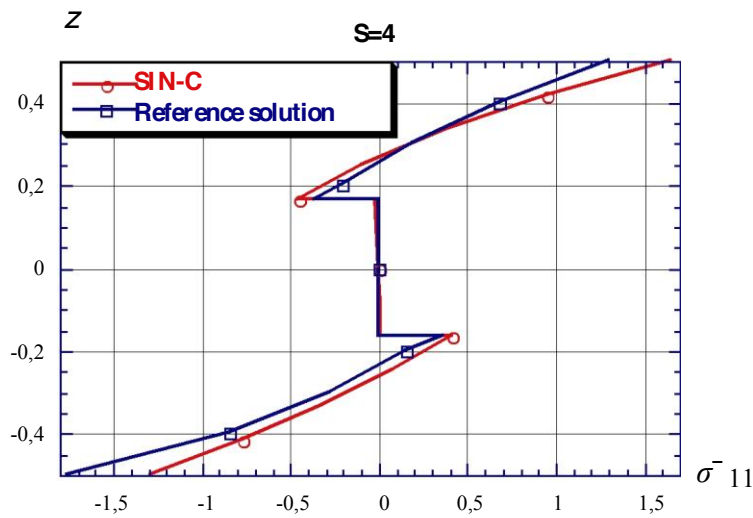


Fig. 9. Three layers case - $\sigma^-_{11}(\Phi/2, L/2, 0)$ distributions for ratio $R/a = 3/\pi$ and $S = 4$.

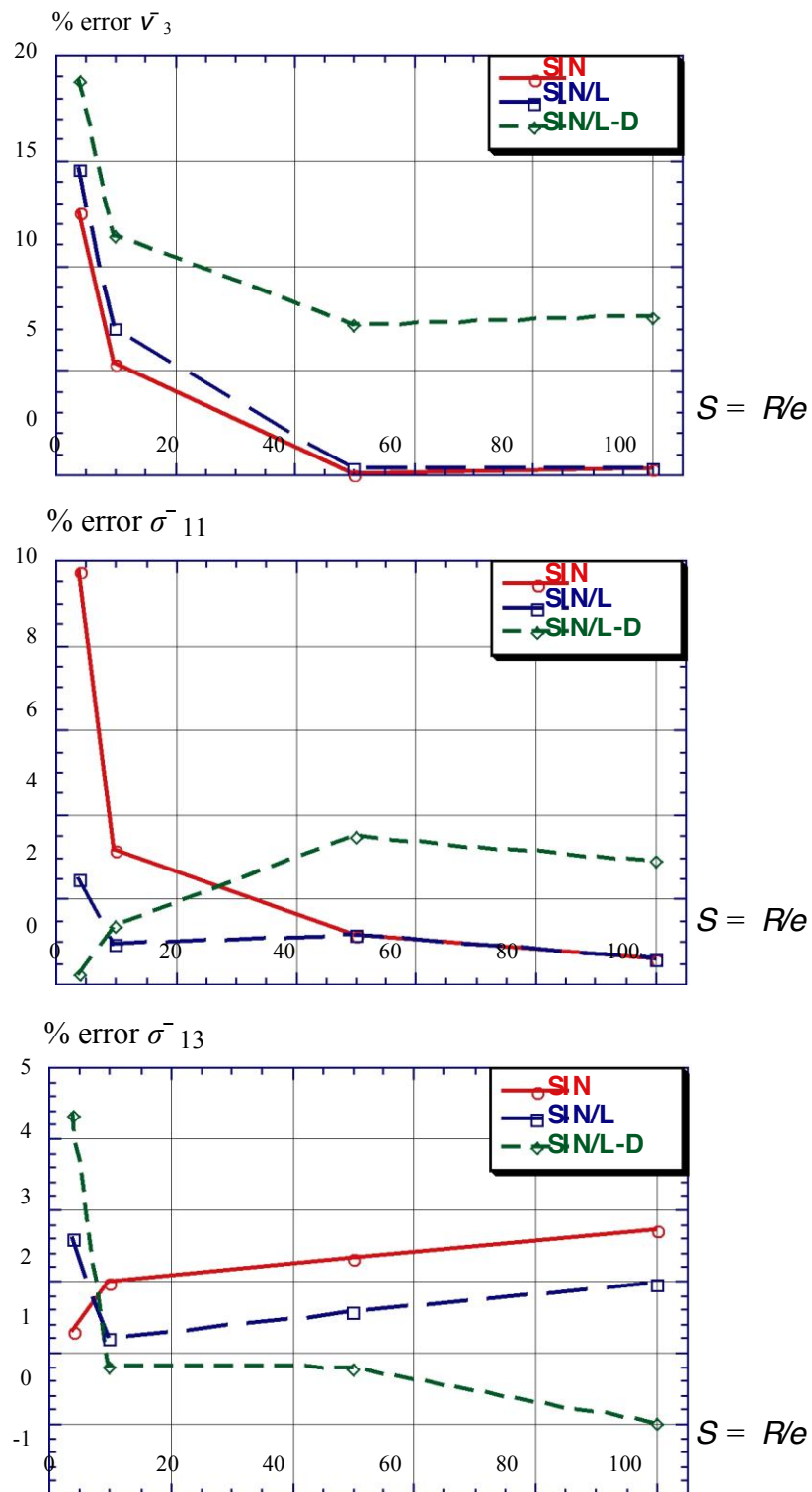


Fig. 10. Homogeneous case ; ratio $R/a = 6/\pi$. Comparisons between SIN, SIN/L, SIN/L-D models

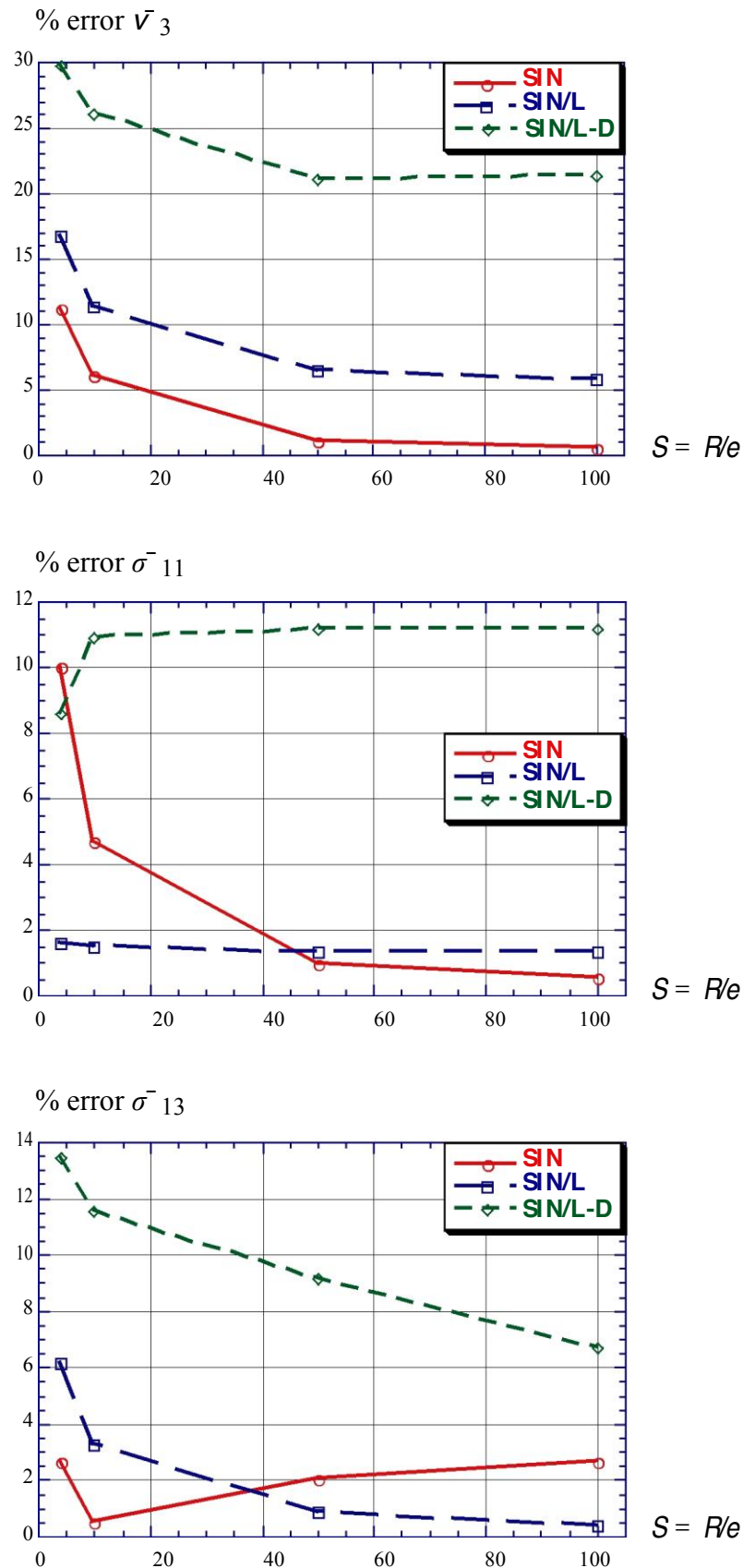


Fig. 11. Homogeneous case ; ratio $R/a = 3/\pi$ ($R/a \sim 1$). Comparisons between SIN, SIN/L, SIN/L-D models.

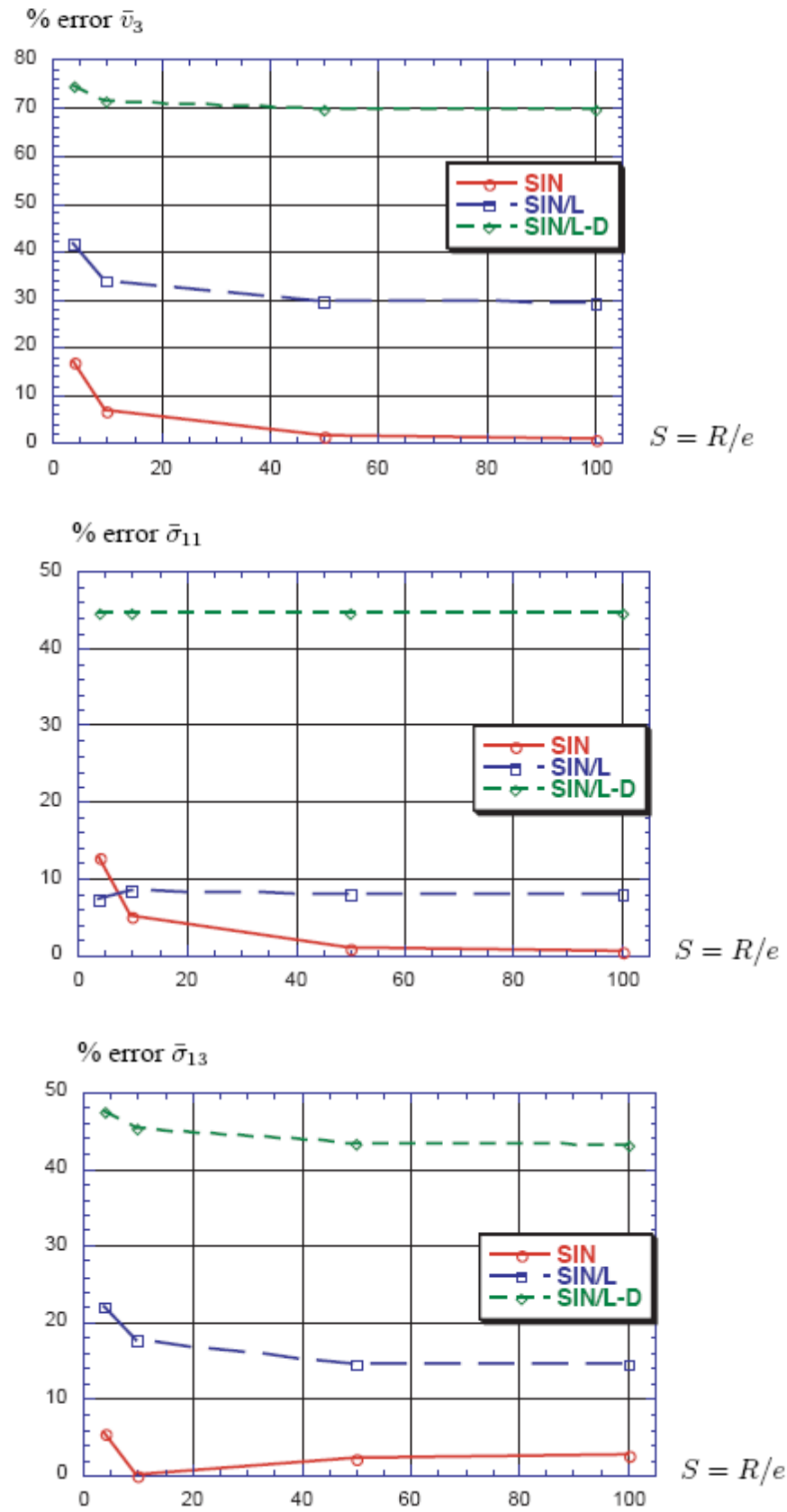


Fig. 12. Homogeneous case ; ratio $R/a = 3/2\pi$. Comparisons between SIN, SIN/L, SIN/L-D models.

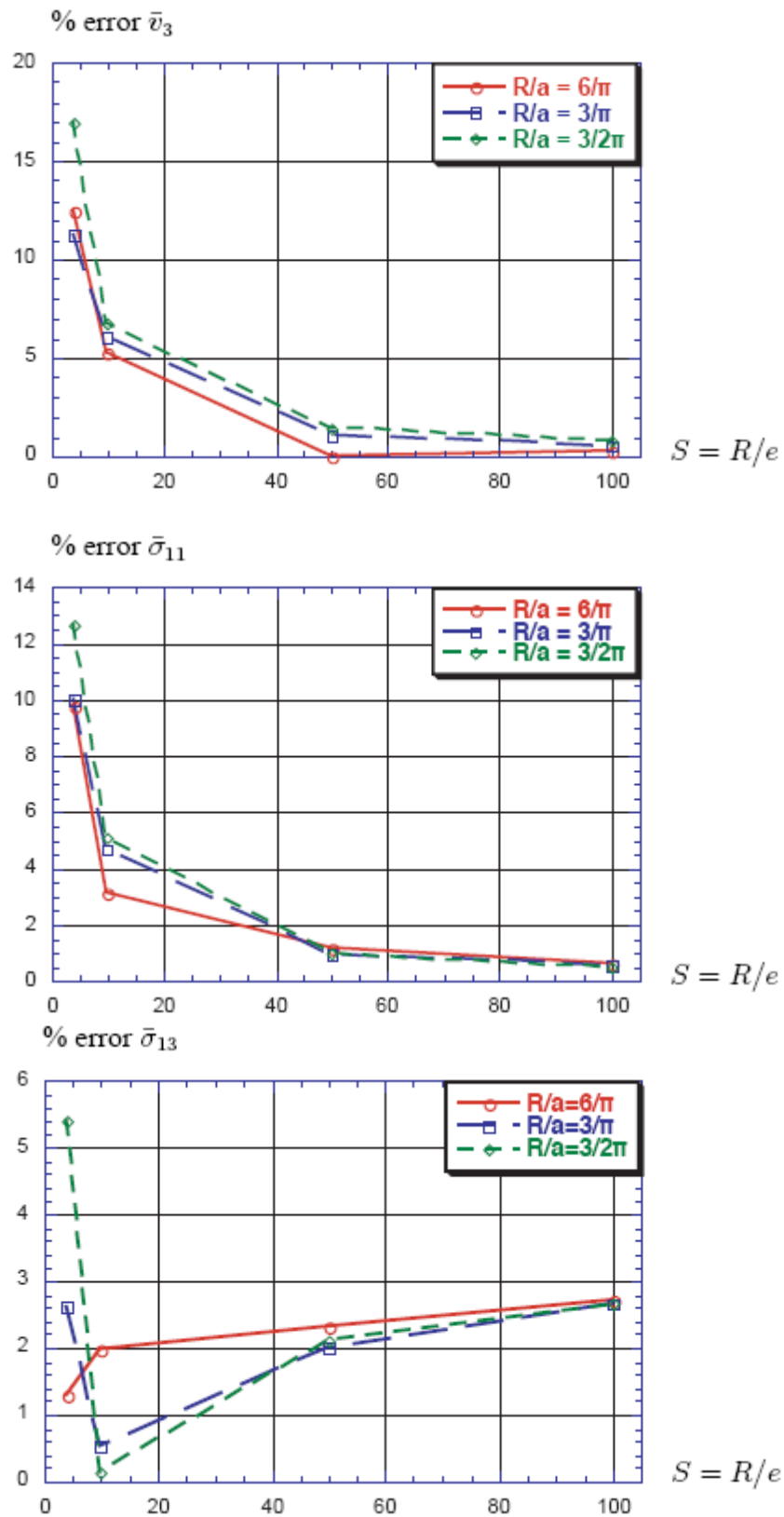


Fig. 13. Homogeneous case-SIN model performances when $R/a = 6/\pi, 3/\pi, 3/2\pi$ and $S = 4, 10, 50, 100$

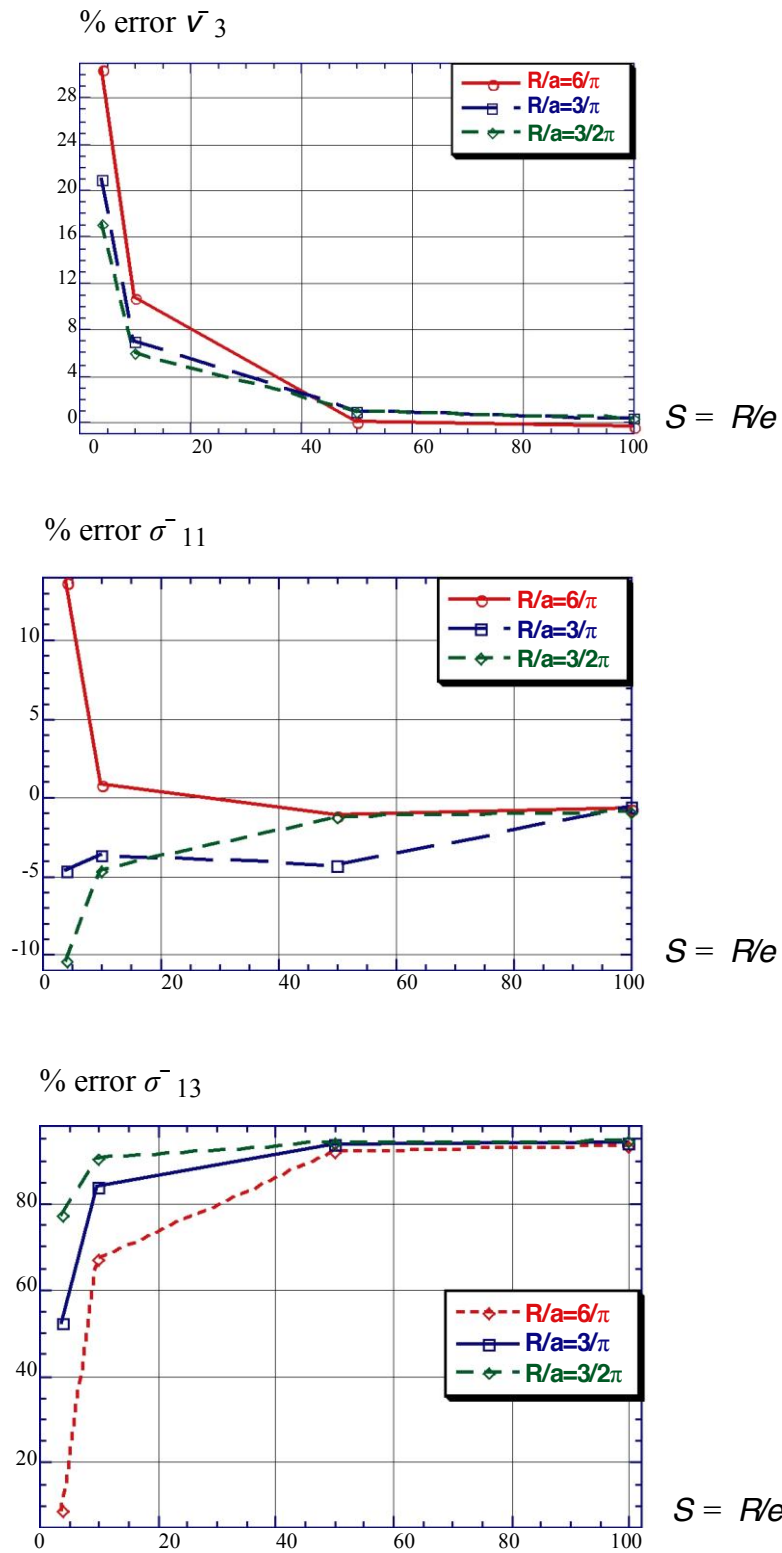


Fig. 14. Two layers case - SIN model performances when $R/a=6/\pi, 3/\pi, 3/2\pi$ and $S = 4, 10, 50, 100$.

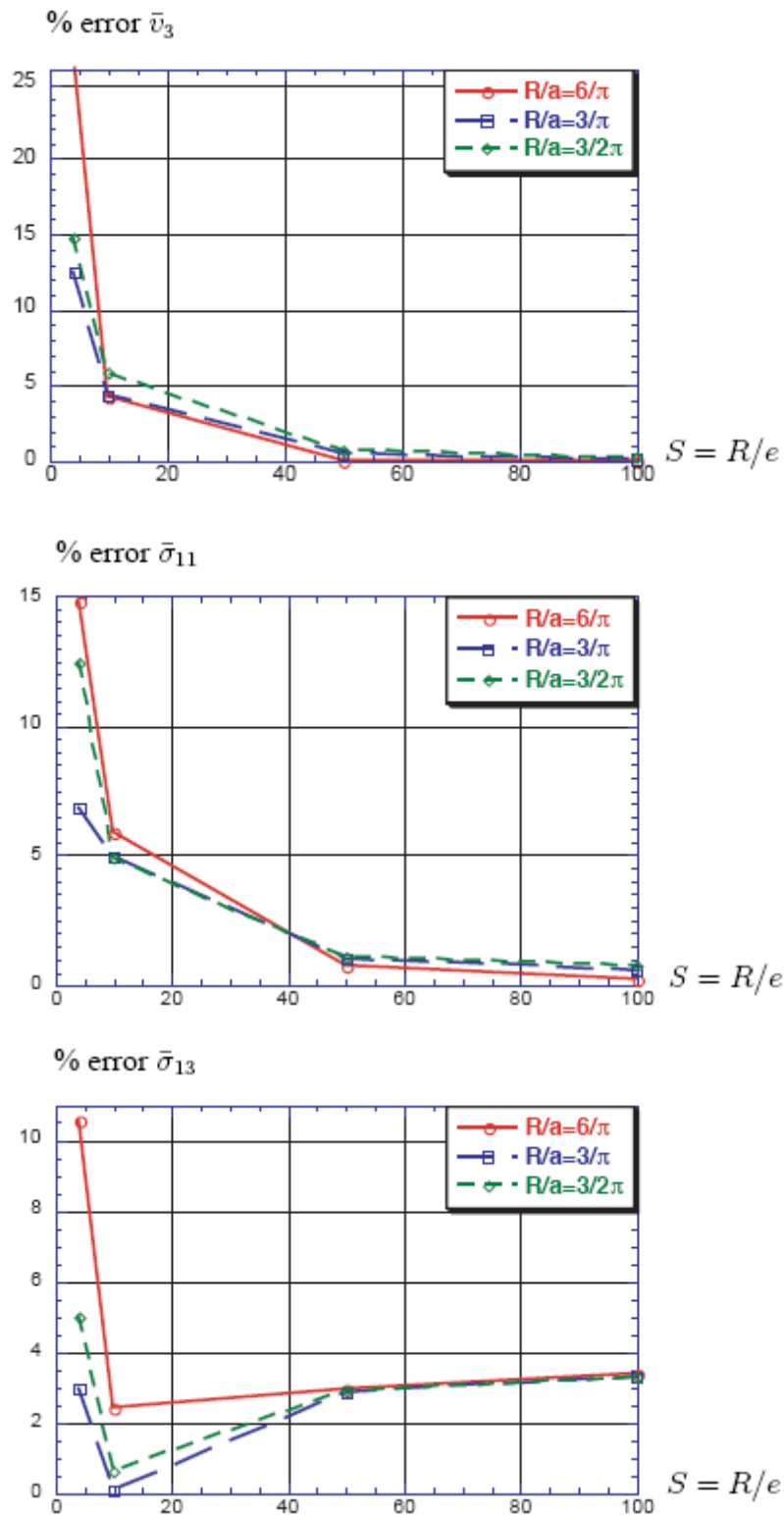


Fig. 15. Three layers case – Relative errors on $\bar{v}_3(\Phi/2, L/2, 0)$, $\bar{\sigma}_{11}(\Phi/2, L/2, -e/2)$ and $\bar{\sigma}_{13}(\Phi, L/2, 0)$.

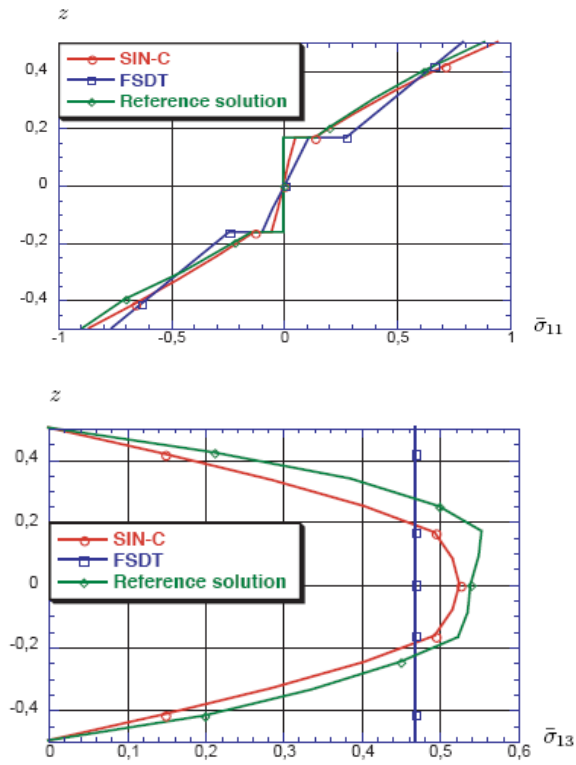


Fig. 16. Three layers case - $\bar{\sigma}_{11}$ and $\bar{\sigma}_{13}$ distributions- $R/a = 3/\pi$ and $S = 10$.

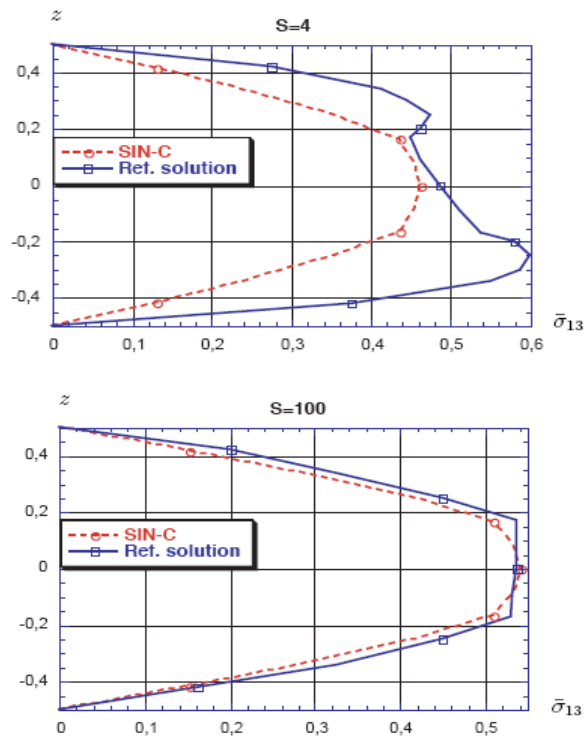


Fig. 17. Three layers case - $\bar{\sigma}_{13}(\Phi, L/2, 0)$ distributions for ratio $R/a = 3/\pi$ and $S = 4, 100$.

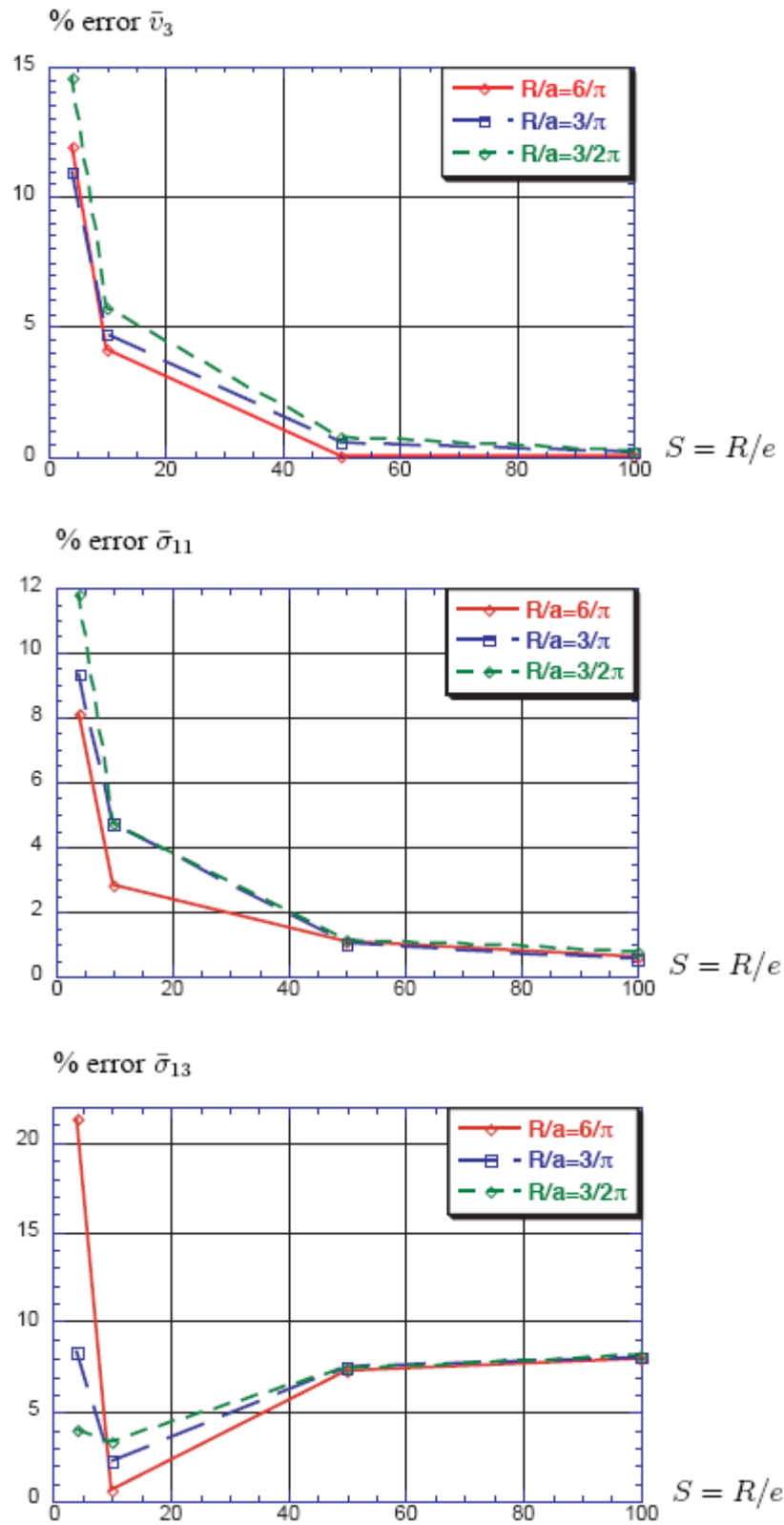


Fig. 18. Five layers case –Relative errors on $\bar{v}_3(\Phi/2, L/2, 0)$, $\bar{\sigma}_{11}(\Phi/2, L/2, -e/2)$ and $\bar{\sigma}_{13}(\Phi, L/2, 0)$.

Model	Strain components in contravariant a^i basis
SIN-C	$2z_{\alpha\beta} = 1/\mu (\varepsilon_{\alpha\beta}^0 + \varepsilon_{\beta\alpha}^0 + F_{\alpha}^v(z) \varepsilon_{v\beta}^1 + F_{\beta}^v(z) \varepsilon_{v\alpha}^1 + G_{\alpha}^v(z) \varepsilon_{v\beta}^2 + G_{\beta}^v(z) \varepsilon_{v\alpha}^2$ $+ z((b_{\beta}^{\lambda} - 2H\delta_{\beta}^{\lambda})(\varepsilon_{\alpha\lambda}^0 + F_{\alpha}^v(z) \varepsilon_{v\lambda}^1 + G_{\alpha}^v(z) \varepsilon_{v\lambda}^2) +$ $(b_{\alpha}^{\lambda} - 2H\delta_{\alpha}^{\lambda})(\varepsilon_{\beta\lambda}^0 + F_{\beta}^v(z) \varepsilon_{v\lambda}^1 + G_{\beta}^v(z) \varepsilon_{v\lambda}^2)))$ $2\varepsilon_{\alpha 3} = F_{\alpha}^{v'}(z)\gamma_v^0$ <p>with $\varepsilon_{\alpha\beta}^0, \varepsilon_{\alpha\beta}^1, \varepsilon_{\alpha\beta}^2$ et γ_v^0 defined in Eq. (15)</p>
SIN-C/L	$2\varepsilon_{\alpha\beta} = \varepsilon_{\alpha\beta}^0 + \varepsilon_{\beta\alpha}^0 + F_{\alpha}^v(z) \varepsilon_{v\beta}^1 + F_{\beta}^v(z) \varepsilon_{v\alpha}^1 + G_{\alpha}^v(z) \varepsilon_{v\beta}^2 + G_{\beta}^v(z) \varepsilon_{v\alpha}^2$ $2\varepsilon_{\alpha 3} = F_{\alpha}^{v'}(z)\gamma_v^0$ <p>with $\varepsilon_{\alpha\beta}^2 = \nu_{3 \alpha\beta}$ and $\varepsilon_{\alpha\beta}^0, \varepsilon_{\alpha\beta}^1, \gamma_v^0$ unchanged</p>
SIN-C/L-D	$2\varepsilon_{\alpha\beta} = \varepsilon_{\alpha\beta}^0 + \varepsilon_{\beta\alpha}^0 + F_{\alpha}^v(z) \varepsilon_{v\beta}^1 + F_{\beta}^v(z) \varepsilon_{v\alpha}^1 + G_{\alpha}^v(z) \varepsilon_{v\beta}^2 + G_{\beta}^v(z) \varepsilon_{v\alpha}^2$ $2\varepsilon_{\alpha 3} = F_{\alpha}^{v'}(z)\gamma_v^0$ <p>with $\gamma_v^0 = \beta_v + \nu_{3,v}$, $\varepsilon_{\alpha\beta}^2 = \nu_{3 \alpha\beta}$ and $\varepsilon_{\alpha\beta}^0, \varepsilon_{\alpha\beta}^1$ unchanged</p>

Table 1 Strains expressions for simplified models.

S= R/e	R/a	6/π			3/π			3/2π					
	Models	\bar{V}_3	$\bar{\sigma}_{11}$	$\bar{\sigma}_{13}$	\bar{V}_3	$\bar{\sigma}_{11}$	$\bar{\sigma}_{13}$	\bar{V}_3	$\bar{\sigma}_{11}$	$\bar{\sigma}_{13}$			
4	Ref. Sol.	0.048	0.427	0.450	0.231	0.312	1.331	1.079	0.572	6.216	6.928	5.397	1.943
	SIN	0.042	0.526	0.409	0.228	0.277	1.248	0.971	0.557	5.199	6.081	4.715	1.838
	SIN/L	0.041	0.474	0.465	0.225	0.260	1.140	1.096	0.537	3.671	5.2794	5.012	1.518
	SIN/L-D	0.039	0.454	0.455	0.221	0.219	0.986	0.987	0.495	1.604	3.001	2.992	1.021
10	Ref. Sol.	0.0112	0.238	0.221	0.253	0.115	0.890	0.807	0.579	3.643	5.415	4.900	1.877
	SIN	0.0108	0.236	0.214	0.258	0.108	0.849	0.769	0.576	3.409	5.142	4.653	1.854
	SIN/L	0.0106	0.227	0.223	0.256	0.102	0.813	0.795	0.560	2.431	4.596	4.493	1.549
	SIN/L-D	0.0101	0.218	0.219	0.251	0.085	0.719	0.720	0.512	1.052	2.720	2.720	1.030
50	Ref. Sol.	0.0042	0.177	0.174	0.259	0.0770	0.768	0.752	0.568	3.111	4.901	4.804	1.818
	SIN	0.0042	0.175	0.172	0.265	0.0762	0.757	0.747	0.580	3.078	4.846	4.765	1.857
	SIN/L	0.0041	0.173	0.172	0.263	0.0720	0.743	0.744	0.563	2.198	4.437	4.427	1.555
	SIN/L-D	0.0039	0.168	0.169	0.257	0.0602	0.666	0.670	0.516	0.950	2.667	2.672	1.032
100	Ref. Sol.	0.0040	0.174	0.172	0.258	0.0755	0.758	0.751	0.565	3.083	4.849	4.801	1.809
	SIN	0.0039	0.172	0.171	0.265	0.0751	0.749	0.752	0.580	3.068	4.815	4.793	1.857
	SIN/L	0.0039	0.171	0.171	0.263	0.0711	0.738	0.746	0.563	2.191	4.426	4.434	1.555
	SIN/L-D	0.0037	0.167	0.167	0.258	0.0594	0.663	0.671	0.516	0.947	2.665	2.673	1.032

Table 2: Results for homogeneous Ren cylindrical panel – Adimensionned displacements and stresses for ratios $R/a=6/\pi, 3/\pi, 3/2\pi$ and $S=R/e=4, 10, 50, 100$.

	R/a	6/π				3/π				3/2π			
S = e	Model	\bar{v}_3	$\bar{\sigma}_{11}$	$\bar{\sigma}_{13}$	\bar{v}_3	$\bar{\sigma}_{11}$	$\bar{\sigma}_{13}$	\bar{v}_3	$\bar{\sigma}_{11}$	$\bar{\sigma}_{13}$	\bar{v}_3	$\bar{\sigma}_{11}$	$\bar{\sigma}_{13}$
4	Ref. Sol.	0.0929	0.1086	0.7490	0.1406	0.8535	0.3840	2.5110	0.3022	24.7960	2.2156	15.0096	0.9350
	SIN-C	0.0676	0.0476	0.7703	0.1836	0.6889	0.2632	2.4038	0.4411	21.1539	1.7863	13.6450	1.4458
	FSDT	0.0873	0.0641	0.4427	0.2423	0.7546	0.2806	1.9361	0.5291	21.4741	1.7981	12.3912	1.6919
	CST	0.0237	0.0640	0.4409		0.4512	0.2800	1.9299		18.3712	1.7973	12.3669	
10	Ref. Sol.	0.0336	0.0688	0.5371	0.1211	0.4931	0.2772	2.2452	0.2559	18.6367	1.7303	14.2125	0.8097
	SIN-C	0.0299	0.0547	0.5372	0.2017	0.4607	0.2498	2.1676	0.4479	17.6764	1.6172	13.5900	1.4397
	FSDT	0.0323	0.0575	0.4713	0.2420	0.4690	0.2519	2.0632	0.5289	16.1384	1.6147	13.2200	1.6935
	CST	0.0221	0.0575	0.4711		0.4204	0.2519	2.0622		17.1506	1.6149	13.2150	
50	Ref. Sol.	0.0217	0.0552	0.4959	0.1076	0.4087	0.2404	2.1655	0.2349	16.6814	1.5368	13.8531	0.7511
	SIN-C	0.0214	0.0543	0.4928	0.2061	0.4057	0.2376	2.1474	0.4509	16.5672	1.5202	13.7632	1.4444
	FSDT	0.0215	0.0544	0.4885	0.2434	0.4055	0.2375	2.1362	0.5320	16.5434	1.5190	13.7036	1.7032
	CST	0.0211	0.0544	0.4886		0.4035	0.2375	2.1363		16.5230	1.5190	13.7036	
100	Ref. Sol.	0.0211	0.0542	0.4936	0.1064	0.4031	0.2369	2.1583	0.2326	16.4967	1.5156	13.8117	0.7443
	SIN-C	0.0210	0.0540	0.4923	0.2062	0.4023	0.2357	2.1503	0.4506	16.4648	1.5077	13.8270	1.4498
	FSDT	0.0211	0.0540	0.4907	0.2435	0.4020	0.2357	2.1454	0.5319	16.4517	1.5070	13.7980	1.7079
	CST	0.0209	0.0540	0.4907		0.4015	0.2356	2.1454		16.4461	1.5070	13.7980	

Table 3: Two layers case – Comparisons of SIN-C, FSDT and CST models. Ratios $R/a=6/\pi, 3/\pi, 3/2\pi$ and $S=R/e=4, 10, 50, 100$.

S = R/e	R/a	6/π				3/π				3/2π			
	Model	\bar{v}_3	$\bar{\sigma}_{11}$	$\bar{\sigma}_{13}$	\bar{v}_3	$\bar{\sigma}_{11}$	$\bar{\sigma}_{13}$	\bar{v}_3	$\bar{\sigma}_{11}$	$\bar{\sigma}_{13}$			
4	Ref. Sol.	0.0693	0.6125	0.5875	0.1654	0.4581	1.7715	1.3671	0.4757	8.0750	8.0003	6.1251	1.7452
	SIN-C	0.0601	0.6974	0.5424	0.1479	0.4009	1.6504	1.2827	0.4617	6.8803	7.0056	5.4240	1.6583
	FSDT	0.0511	0.2116	0.1462	0.0877	0.3478	0.9247	0.6381	0.1913	5.9578	5.9422	4.0823	0.6136
	CST	0.0420	0.2117	0.1463		0.0781	0.9189	0.6346		3.2325	5.9359	4.0700	
10	Ref. Sol.	0.0163	0.3020	0.2736	0.2176	0.1440	0.9949	0.8972	0.5251	4.0411	5.7250	5.1919	1.7296
	SIN-C	0.0156	0.2983	0.2699	0.2229	0.1377	0.9458	0.8552	0.5247	3.8036	5.4437	4.9190	1.7186
	FSDT	0.0132	0.1907	0.1646	0.0877	0.1221	0.8330	0.7184	0.1913	3.6355	5.3523	4.6120	0.6146
	CST	0.0042	0.1909	0.1648		0.0777	0.8321	0.7178		3.1993	5.3523	4.6130	
50	Ref. Sol.	0.0046	0.1860	0.1824	0.2390	0.0808	0.7982	0.7831	0.5253	3.2361	5.0836	4.9880	1.6831
	SIN-C	0.0046	0.1840	0.1805	0.2461	0.0804	0.7902	0.7753	0.5404	3.2129	5.0284	4.9444	1.7317
	FSDT	0.0045	0.1801	0.1750	0.0878	0.0798	0.7887	0.7666	0.1922	3.2060	5.0436	4.9128	0.6153
	CST	0.0041	0.1801	0.1751		0.0776	0.0089	0.0066		3.1885	5.0436	4.9128	
100	Ref. Sol.	0.0042	0.1807	0.1789	0.2390	0.0786	0.7866	0.7791	0.5234	3.1996	5.0278	4.9804	1.6754
	SIN-C	0.0042	0.1796	0.1781	0.2471	0.0785	0.7824	0.7758	0.5407	3.1937	4.9915	4.9709	1.7306
	FSDT	0.0042	0.1789	0.1765	0.0878	0.0783	0.7829	0.7726	0.1919	3.1919	5.0011	4.9569	0.6147
	CST	0.0041	0.1787	0.1765		0.0779	0.7828	0.7727		3.1876	5.0010	4.9572	

Table 4: Three layers case – Comparisons of SIN-C, FSDT and CST models. Ratios $R/a=6/\pi, 3/\pi, 3/2\pi$ and $S=RE=4,10,50,100$.

S = R/e	R/a	6/π				3/π				3/2π			
		Model	\bar{v}_3	$\bar{\sigma}_{11}$	$\bar{\sigma}_{13}$	\bar{v}_3	$\bar{\sigma}_{11}$	$\bar{\sigma}_{13}$	\bar{v}_3	$\bar{\sigma}_{11}$	$\bar{\sigma}_{13}$		
4	Ref. Sol.	0.0763	0.6444	0.5904	0.2608	0.4834	1.7808	1.3920	0.5512	8.6511	8.7093	6.7994	1.7406
	SIN-C	0.0672	0.6964	0.5417	0.2051	0.4306	1.6147	1.2555	0.5053	7.3945	7.6825	5.9626	1.6718
	FSDT	0.0637	0.2538	0.1772	0.2239	0.3760	1.1103	0.7742	0.4893	6.7438	7.1206	4.9536	1.5675
	CST	0.0050	0.2533	0.1768		0.0959	1.1041	0.7698		3.8795	7.1181	4.9420	
10	Ref. Sol.	0.0171	0.3110	0.2839	0.2359	0.1579	1.1214	1.0170	0.5118	4.6838	6.7602	6.1371	1.6341
	SIN-C	0.0164	0.3022	0.2735	0.2345	0.1505	1.0688	0.9659	0.5233	4.4188	6.4436	5.8157	1.6879
	FSDT	0.0144	0.2292	0.1986	0.2236	0.1398	1.0028	0.8676	0.4886	4.3093	6.4407	5.5637	1.5684
	CST	0.0050	0.2291	0.1986		0.0950	1.0012	0.8662		3.8509	6.4424	5.5610	
50	Ref. Sol.	0.0054	0.2214	0.2172	0.2249	0.0967	0.9590	0.9406	0.4918	3.8923	6.1218	6.0005	1.5737
	SIN-C	0.0054	0.2190	0.2148	0.2411	0.0962	0.9494	0.9312	0.5285	3.8641	6.0544	5.9524	1.6912
	FSDT	0.0053	0.2168	0.2108	0.2239	0.0958	0.9500	0.9238	0.4905	3.8597	6.0748	5.9220	1.5705
	CST	0.0050	0.2169	0.2108		0.0940	0.9500	0.9239		3.8413	6.0748	5.9220	
100	Ref. Sol.	0.0050	0.2171	0.2150	0.2237	0.0945	0.9472	0.9381	0.4894	3.8539	6.0581	6.0000	1.5659
	SIN-C	0.0050	0.2158	0.2138	0.2415	0.0944	0.9421	0.9338	0.5285	3.8463	6.0136	5.9878	1.6928
	FSDT	0.0050	0.2155	0.2126	0.2241	0.0943	0.9433	0.9310	0.4906	3.8452	6.0251	5.9737	1.5717
	CST	0.0049	0.2155	0.2126		0.0938	0.9432	0.9310		3.8406	6.0251	5.9738	

Table 5: Five layers case – Comparisons of SIN-C, FSDT and CST models. Ratios $R/a=6/\pi, 3/\pi, 3/2\pi$ and $S=R/e=4, 10, 50, 100$.

A. Details about the refined shell model

• For a layer (k), transverse shear stresses versus strains are expressed by:

$$\begin{cases} \sigma_{13}^{(k)}(\xi_1, \xi_2, z, t) = (\bar{C}_{55}^{(k)} f_1'(z) + a_{55}^{(k)}) \gamma_1^0(\xi_1, \xi_2, t) + (\bar{C}_{45}^{(k)} f_2'(z) + a_{54}^{(k)}) \gamma_2^0(\xi_1, \xi_2, t) \\ \sigma_{23}^{(k)}(\xi_1, \xi_2, z, t) = (\bar{C}_{45}^{(k)} f_1'(z) + a_{45}^{(k)}) \gamma_1^0(\xi_1, \xi_2, t) + (\bar{C}_{44}^{(k)} f_2'(z) + a_{44}^{(k)}) \gamma_2^0(\xi_1, \xi_2, t) \end{cases} \quad (A.1)$$

Where,

$$f_1'(z) = f'(z) - \frac{e}{\pi} b_{55} f''(z) \quad (\text{A.2})$$

$$f_2'(z) = f'(z) - \frac{e}{\pi} b_{44} f''(z)$$

with $f_3(z) = df(z)/dz$ et $f_{33}(z) = d^2f(z)/dz^2$, first and second derivatives of Sinus shear function $f(z)$. γ_1^0 and γ_2^0 standing for the two transverse shear strains on the middle surface of the shell.

Reduced elastic coefficients $\bar{C}_{ij}^{(k)}$ including $\sigma_{zz} = 0$ hypothesis are given by:

$$\begin{cases} \bar{C}_{ij}^{(k)} = C_{ij}^{(k)} - C_{i3}^{(k)} C_{j3}^{(k)} / C_{33}^{(k)} \text{ pour } i, j = 1; 2; 6 \\ \bar{C}_{ij}^{(k)} = C_{ij}^{(k)} \text{ pour } i, j = 4, 5 \end{cases} \quad (\text{A.3})$$

where $C_{ij}^{(k)}$ are 3D elastic coefficients before including $\sigma_{33} = 0$. Symmetric or un-symmetric monoclinic layers can be considered in Eq. (A.1) and Eq. (A.3).

On the other hand, a_{44} , a_{45} , a_{54} , a_{55} and b_{44} , b_{55} coefficients in Eq. (A.1) and Eq. (A.2) are introduced to satisfy transverse shear stresses $\sigma_{\alpha 3}$ continuity at inter layers and on top and bottom faces of the shell.

- The next step consists in considering the transverse strains α_3 given in [32,11] for shallow shells:

$$2\epsilon_{\beta 3}^{(k)} = v_{3,\beta} + u_{\beta,3}^{(k)} \quad (\text{A.4})$$

Using flexibility material coefficients S_{ij} , for $(i, j)=(4,5)$, α_3 can be written as:

$$\begin{cases} 2\epsilon_{13}^{(k)} = S_{55}^{(k)} \sigma_{13}^{(k)} + S_{45}^{(k)} \sigma_{23}^{(k)} \\ 2\epsilon_{23}^{(k)} = S_{45}^{(k)} \sigma_{13}^{(k)} + S_{44}^{(k)} \sigma_{23}^{(k)} \end{cases} \quad (\text{A.5})$$

- From Eq. (A.4) and Eq. (A.5) and by respect of $\sigma_{\alpha 3}(k)$ distribution given in Eq.

(A.1), it can be easily deduced:

$$\begin{cases} u_{1,3}^{(k)} = -v_{3,1} + (f_1'(z) + S_{55}^{(k)} a_{55}^{(k)} + S_{45}^{(k)} a_{45}^{(k)}) \gamma_1^0 \\ \quad + (S_{55}^{(k)} a_{54}^{(k)} + S_{45}^{(k)} a_{44}^{(k)}) \gamma_2^0 \\ u_{2,3}^{(k)} = -v_{3,2} + (S_{44}^{(k)} a_{45}^{(k)} + S_{45}^{(k)} a_{55}^{(k)}) \gamma_1^0 + \\ \quad (f_2'(z) + S_{44}^{(k)} a_{44}^{(k)} + S_{45}^{(k)} a_{54}^{(k)}) \gamma_2^0 \end{cases} \quad (\text{A.6})$$

or

$$\begin{cases} u_{1,3}^{(k)} = -v_{3,1} + (f_1'(z) + a_1^{(k)}) \gamma_1^0 + (a_2^{(k)}) \gamma_2^0 \\ u_{2,3}^{(k)} = -v_{3,2} + (a_3^{(k)}) \gamma_1^0 + (f_2'(z) + a_4^{(k)}) \gamma_2^0 \end{cases} \quad (\text{A.7})$$

putting down,

$$a_1^{(k)} = S_{55}^{(k)} a_{55}^{(k)} + S_{45}^{(k)} a_{45}^{(k)} \quad a_2^{(k)} = S_{55}^{(k)} a_{54}^{(k)} + S_{45}^{(k)} a_{44}^{(k)} \quad (\text{A.8})$$

$$a_3^{(k)} = S_{44}^{(k)} a_{45}^{(k)} + S_{45}^{(k)} a_{55}^{(k)} \quad a_4^{(k)} = S_{44}^{(k)} a_{44}^{(k)} + S_{45}^{(k)} a_{54}^{(k)}$$

- Finally, bending and transverse shear components of displacement can be obtained by integration of Eq. (A.7) according to z-co-ordinate.

Adding $\mu^p_a v_p$ so that classical Koiter model could be retrieved, the final displacement field can be achieved:

$$\begin{cases} u_1(\xi^1, \xi^2, z, t)^{(k)} = \mu_1^\alpha v_\alpha(\xi^1, \xi^2, t) - z v_{3,1}(\xi^1, \xi^2, t) + F_1^{\alpha(k)}(z) \gamma_\alpha^0(\xi^1, \xi^2, t) \\ u_2(\xi^1, \xi^2, z, t)^{(k)} = \mu_2^\alpha v_\alpha(\xi^1, \xi^2, t) - z v_{3,2}(\xi^1, \xi^2, t) + F_2^{\alpha(k)}(z) \gamma_\alpha^0(\xi^1, \xi^2, t) \\ u_3(\xi^1, \xi^2, z, t)^{(k)} = v_3(\xi^1, \xi^2, t) \end{cases} \quad (\text{A.9})$$

with

$$\begin{aligned} F_1^{1(k)}(z) &= f_1(z) + g_1^{(k)}(z); & F_1^{2(k)}(z) &= g_2^{(k)}(z) \\ F_2^{1(k)}(z) &= g_3^{(k)}(z); & F_2^{2(k)}(z) &= f_2(z) + g_4^{(k)}(z) \end{aligned} \quad (\text{A.10})$$

Thickness functions $g(k)1(z), \dots, g(k)4(z)$ are linear functions defined by:

$$g_i^{(k)}(z) = a_i^{(k)} z + d_i^{(k)} \quad i = 1, 2, 3, 4. \quad \text{and} \quad k = 1, 2, 3, \dots, n.$$

depending on $a_i^{(k)}, d_i^{(k)}$ coefficients. $d_i^{(k)}$ allows to ensure displacements continuity at interlayer and on the middle surface of the shell.

Trigonometric functions

$$f_1(z) = f(z) - \frac{e}{\pi} b_{55} f'(z) \quad \text{and} \quad f_2(z) = f(z) - \frac{e}{\pi} b_{44} f'(z)$$

defined through the shell thickness e depend on b_{44} and b_{55} constant.

- Previous coefficients $a_i^{(k)}, d_i^{(k)}$ on one hand and b_{44} and b_{55} on the other hand, are respectively determined from boundary conditions on top and bottom faces of the shell and from both displacements and transverse shear stresses continuity at inter-layer. The identification method is detailed in [11].

B. Details about the reference solution

In this part, the Ren approach is briefly recalled using its own notations.

Step 1: Using (r, θ) as in plane cylindrical coordinates, Fig. 6, constitutive equations are given by:

$$\begin{aligned} \epsilon_{rr} &= R_{11} \sigma_{rr} + R_{12} \sigma_{\theta\theta} \\ \epsilon_{\theta\theta} &= R_{12} \sigma_{rr} + R_{22} \sigma_{\theta\theta} \\ 2\epsilon_{r\theta} &= R_{66} \sigma_{r\theta} \end{aligned} \quad (\text{B.1})$$

where $R_{11}, R_{12}, R_{22}, R_{66}$ are reduced flexibility coefficients obtained putting down $z_z = 0$ (plane strain hypothesis). They are defined by $R_{ij} = S_j - S_3 S_j / S_3$ for $i, j = 1, 2, 6$ where S_j are flexibility coefficients of material.

Step 2: Equilibrium equations without body forces are:

$$\begin{aligned} \frac{\partial \sigma_{rr}}{\partial r} + \frac{1}{r} \frac{\partial \sigma_{r\theta}}{\partial \theta} + \frac{\sigma_{rr} - \sigma_{\theta\theta}}{r} &= 0 \\ \frac{\partial \sigma_{r\theta}}{\partial r} + \frac{1}{r} \frac{\partial \sigma_{\theta\theta}}{\partial \theta} + \frac{2\sigma_{r\theta}}{r} &= 0 \end{aligned} \quad (\text{B.2})$$

and strain relations are defined by:

$$\begin{aligned}\epsilon_{rr} &= \frac{\partial u}{\partial r} \\ \epsilon_{\theta\theta} &= \frac{1}{r} \frac{\partial v}{\partial \theta} + \frac{u}{r} \\ 2\epsilon_{r\theta} &= \frac{1}{r} \frac{\partial u}{\partial \theta} + \frac{\partial v}{\partial r} - \frac{v}{r}\end{aligned}\quad (\text{B.3})$$

u and v are respectively the displacements in the r -direction and θ -direction. Furthermore, the in-plane strain state expressed by $z_z = 0$ involves the additional stresses relation:

$$\sigma_{zz} = -\frac{1}{S_{33}}(S_{13}\sigma_{rr} + S_{23}\sigma_{\theta\theta}) \quad (\text{B.4})$$

Step 3: The $F(r, \theta)$ function is then introduced satisfying Eq.(B.2) and it follows:

$$\begin{aligned}\sigma_{rr} &= \frac{1}{r} \frac{\partial F}{\partial r} + \frac{1}{r^2} \frac{\partial^2 F}{\partial \theta^2} \\ \sigma_{\theta\theta} &= \frac{\partial^2 F}{\partial r^2} \\ \sigma_{r\theta} &= -\frac{\partial^2}{\partial r \partial \theta} \left(\frac{F}{r} \right)\end{aligned}\quad (\text{B.5})$$

Step 4: Issued from Eq. (B.3), the compatibility equation can be written as:

$$\frac{\partial}{\partial r} \left(r \frac{\partial (2\epsilon_{r\theta})}{\partial \theta} \right) = \frac{\partial^2 \epsilon_{rr}}{\partial \theta^2} + 2r \frac{\partial \epsilon_{\theta\theta}}{\partial r} + r^2 \frac{\partial^2 \epsilon_{\theta\theta}}{\partial r^2} - r \frac{\partial \epsilon_{rr}}{\partial r} \quad (\text{B.6})$$

From Eq. (B.6) and constitutive relations Eq. (B.1), the following differential equation must be satisfied by F :

$$\begin{aligned}R_{22} \frac{\partial^4 F}{\partial r^4} + (2R_{12} + R_{66}) \frac{1}{r^2} \frac{\partial^4 F}{\partial r^2 \partial \theta^2} + R_{11} \frac{1}{r^4} \frac{\partial^4 F}{\partial \theta^4} \\ + 2R_{22} \frac{1}{r} \frac{\partial^3 F}{\partial r^3} - (2R_{12} + R_{66}) \frac{1}{r^3} \frac{\partial^3 F}{\partial r \partial \theta^2} - R_{11} \frac{1}{r^2} \frac{\partial^2 F}{\partial r^2} \\ + (2R_{11} + 2R_{12} + R_{66}) \frac{1}{r^4} \frac{\partial^2 F}{\partial \theta^2} + R_{11} \frac{1}{r^3} \frac{\partial F}{\partial r} = 0\end{aligned}\quad (\text{B.7})$$

step 5: Following step consists in finding F function satisfying:

- differential equation Eq. (B.7),
- boundary conditions on the top and bottom surfaces

$$\begin{aligned}\sigma_{rr}(r_o, \theta) &= q(\theta) \\ \sigma_{rr}(r_i, \theta) &= \sigma_{r\theta}(r_i, \theta) = \sigma_{r\theta}(r_o, \theta) = 0\end{aligned}\quad (\text{B.8})$$

where r_i and r_o are respectively inner and outer radius for the cylindrical panel. – simply supported boundary conditions

$$\begin{aligned}\sigma_{\theta\theta}(r, 0) &= \sigma_{\theta\theta}(r, \phi) = 0 \\ u(r, 0) &= u(r, \phi) = 0\end{aligned}\quad (\text{B.9})$$

– interface continuity conditions such that σ_{rr} , $\sigma_{r\theta}$, u and v are equal at each interface. The stress function F is searched under the form:

$$F(r, \theta) = f(r) \sin(k\theta)$$

assuming a pressure loading on the Fourier series form

$$q(\theta) = \sum_{n=1}^{\infty} q_n \sin(k\theta)$$

with $k = \frac{n\pi}{\phi}$, $n = 1, 2, \dots$

$\alpha(\xi^1)$ introduced in Section 4 can be easily related to q_θ putting down $\xi_1 = R\theta$ and $n = 1$.